THEORETICAL STUDIES OF EXCITED STATE ELECTRON TRANSFER BETWEEN IRON-PORPHYRIN AND TRINITROTOLUENE

By

CLINT BRADEN CONNER

Associates of Science
Rogers State University
Claremore, Oklahoma
1998

Bachelor of Science
Northeastern State University
Tahlequah, Oklahoma
2000

Submitted to the Faculty of the
Graduate College of the
Oklahoma State University
in partial fulfillment of
the requirements for
the Degree of
DOCTOR OF PHILOSOPHY
December, 2006

THEORETICAL STUDIES OF
ELECTRON TRANSFER BETWEEN IRON-PORPHYRIN
AND TRINITROTOLUENE

Thesis Approved:

Dr. Timothy M. Wilson
Thesis Advisor

Dr. Harold J. Harmon

Dr. Gil Summy

Dr. Nick Materer

Dr. A. Gordon Emslie
Dean of the Graduate College

ACKNOWLEDGMENTS

I would first like to thank my advisor Dr. Timothy Wilson for all his help during my studies and my research. He has given me a better understanding of the principles governing our research. I have also enjoyed the many conversations outside the realm of physics. His encouragement has helped greatly through my time in graduate school. In times I felt like giving up, unknowing to him, he would always encourage me at just the right time to boost my confidence and keep me sane. I would like to extend my thanks also to my committee members: Dr. Jim Harmon, Dr. Thomas Collins, Dr. Gil Summy, and Dr. Nick Materer; all have pointed me in directions that I might have not considered concerning my research.

I would like to further thank Dr. Jim Harmon for his financial support through my research assistantship. He has given Dr. Wilson and me avenues to explore in our research. I thank him for all the laughs and not putting up with the political correctness. I thank him also for being blunt and not sugar coating the issues discussed.

I want to especially thank Dr. Paul Westhaus for his endless support in my education as one of my professors. His tireless work and great attention to detail in my class work has greatly benefited my education. He has always been willing to help in matters that he didn't have to, thus taking much stress off of me. He always made sure I had a teaching assistantship in the beginnings of my schooling, which I was always grateful for. His help will certainly leave a positive lasting impression in my life.

To my friends I would like to say thank you to Brian Timmons, Lisa Reilly, Enkhbot Tesdinbaljir, Mammadur Rahaman, Kirk Haines, Marty Monigold, and

Ryan Scott for our endless discussion about physics and matters outside of physics. These friends of mine have made graduate school a much more enjoyable time when it would have otherwise been extremely stressful. Thank you all for your support and help that you have given me every step of the way. On the same note I would like to thank another friend Tate Pope for his great conversation on religion and science. He has on many occasions opened my mind and caused me to understand why I hold the beliefs I do.

To the office staff in the physics department consisting of Cindi Raymond, Susan Cantrell, and Stephanie Hall I say thank you for your help in all that you do. All of you are some of the hardest working folks I have had the pleasure of getting to know and enjoy. Thank you for making sure I got paid, had the right books to check out, and had all the correct information for travelling to various locations.

Lastly, I thank my mom, dad, step dad, and the rest of my family for their moral and financial support, as well as the endless encouragement they continuously gave me through throughout my entire schooling. You all have been their in every occasion and then some. Thank you for caring and making sure that I finished what I started.

TABLE OF CONTENTS

Chapter Page

1. INTRODUCTION 1

1.1. History 1
1.2. Outline of Thesis 4

2. THEORY 6

2.1. Introduction 6
2.2. Hartree-Fock 6
2.2.1. Basis Sets 9
2.3. Density Functional Theory 12
2.4. Time-Dependent Density Functional Theory 15
2.5. Configuration Interaction 18
2.6. Polarizable-Continuum Model 19

3. CALCULATIONS 21

3.1. Introduction 21
3.2. Unsolvated FeP and FeTPP Complexes 22
3.2.1. Geometry Optimization FeP 22
3.2.2. Geometry Optimization FeTPP 26
3.3. Unsolvated Excited States of FeP and FeTPP 29
3.3.1. Unsolvated FeP Excited States 29
3.3.2. Unsolvated FeTPP Excited States 38
3.3.3. Charge and Spin Densities of Unsolvated FeP and FeTPP 42
3.3.4. Comparison of Unsolvated FeP and FeTPP . . . 43
3.4. Solvated FeP Complexes 44
3.4.1. FeP Excited States 44
3.4.2. Solvated FeP Spin and Charge Densities 47

Chapter Page
4. Excited State Electron Transfer 49

4.1. Introduction 49
4.2. Thermodynamic Factors of Photoinduced Electron Transfer 52
4.2.1. Quenchers and Sensitizers 52
4.2.2. Enthalpy and Gibbs Free Energy 53
4.2.3. Redox Potentials 55

5. Excited State Electron Transfer Results 60

5.1. Introduction 60
5.2. Calculations 61
5.3. Thermodynamic Calculations 64

6. Summary and Conclusion 71

BIBLIOGRAPHY 73

LIST OF TABLES

Table		Page
3.1.	Table giving the optimized total energies of the FeP and FeTPP multiplet system.	23
3.2.	Table showing the optimized bond lengths of the FeP multiplet system.	24
3.3.	Table giving the optimized parameters of the FeP multiplet system.	25
3.4.	Table showing the optimized bond lengths of the FeTPP triplet and quintet system.	27
3.5.	Table giving the optimized parameters of the FeTPP triplet and quintet system.	28
3.6.	Table giving the TDDFT excitation data for the S=1 system of FeP.	30
3.7.	Table giving the CIS excitation data for the S=1 system of FeP.	31
3.8.	Table giving the TDDFT excitation data for the S=2 system of FeP.	32
3.9.	Table giving the CIS excitation data for the S=2 system of FeP.	33
3.10.	Table giving the TDDFT excitation data for the S=0 system of FeP.	34
3.11.	Table giving the TDDFT excitation data for the S=1 system of FeP and the experimental results of FeTPP in benzene.	37
3.12.	Table giving the TDDFT excitation data for the S=1 system of FeTPP.	39
3.13.	Table giving the TDDFT excitation data for the S=2 system of FeTPP.	40
3.14.	Table giving the TDDFT excitation data for the S=1 system of FeTPP and the experimental results of FeTPP in benzene.	41
3.15.	Table giving the Mulliken charge densities and spin densities the triplet FeTPP and FeP.	42

Table Page
3.16. Table giving the TDDFT excitation data for the solvated S=1 system of FeP. 45

3.17. Table giving the TDDFT excitation data for the solvated S=2 system of FeP. 46

3.18. Table giving the Mulliken charge densities and spin densities the triplet and quintet FeP. 48

5.1. Table giving the occupied orbitals of the FeP and FeP^{+1} complexes. . 64

5.2. Table giving the Gibbs free energies for each molecule. 69

5.3. Table giving the change in free energies for each set of reactions. . . . 69

LIST OF FIGURES

Figure Page

1.1. Model of FeP molecule. This model is used as a reference diagram for the optimized parameters. 2

1.2. Model of FeTPP molecule. This model is used as a reference diagram for the optimized parameters. 3

2.1. Pictographs of the functions used to describe the orbitals. 11

3.1. Absorbance spectrum of 6.7 μM FeTPPS in pH 7 buffer. Inset are the Q-bands of FeTPPS. 35

4.1. Excitation of the electron to the Frank-Condon state which then relaxes to the equilibrated state. 51

4.2. Enthalpy changes of the donor complex. 54

4.3. Energy diagram for photoinduced electron transfer. 57

5.1. Model of solvated FeP triplet charge density map. This model is used as a reference diagram for the atomic charges. 62

5.2. Model of solvated FeP S=3/2 charge density map. This model is used as a reference diagram for the atomic charges. 63

5.3. Model of solvated TNT S=0 charge density map. This model is used as a reference diagram for the atomic charges. 65

5.4. Model of solvated ionic TNT S=1/2 charge density map. This model is used as a reference diagram for the atomic charges. 66

CHAPTER 1

INTRODUCTION

1.1 History

The study of porphyrins and porphyrin complexes is extensive due to their biological importance, as well as their use in industrial applications and devices. Some of these include their use as optical limiters, catalysts, sensors, actuators, and molecular sieves.[1] Two particular types of porphyrin of interest, shown in Figures 1.1 and 1.2, are those of the iron(II)-porphyrin (FeP) and iron(II)-tetraphenylporphyrin (FeTPP), which have been studied extensively.

Much research has been performed on both FeP and FeTPP by many different research groups. In these studies the actual ground state of the FeP system was questioned in earlier work, centering on whether the ground state of the system was an S=0, 1, or 2 for the d^6 iron(II) complex.[2–4] Numerous theoretical studies have addressed this ambiguity and most have concluded computationally that the S=1 spin state is energetically favorable over the other spins for the ground state.[5–7] Experimentally, there is still some question as to the exact ground state of the d^6 FeP. Like the computational studies for FeP, the experimental studies seek to determine the ground state of the system by using various methods including: observing their magnetic moments of iron(II)-tetraphenyl-porphyrin (FeTPP); measuring Fe-N bond distances in FeTPP [8]; and Mössbauer [8,9] and NMR spectroscopy of FeTPP [10] to name a few. In each case the ground state was suggested by the data to be of intermediate spin, S=1.

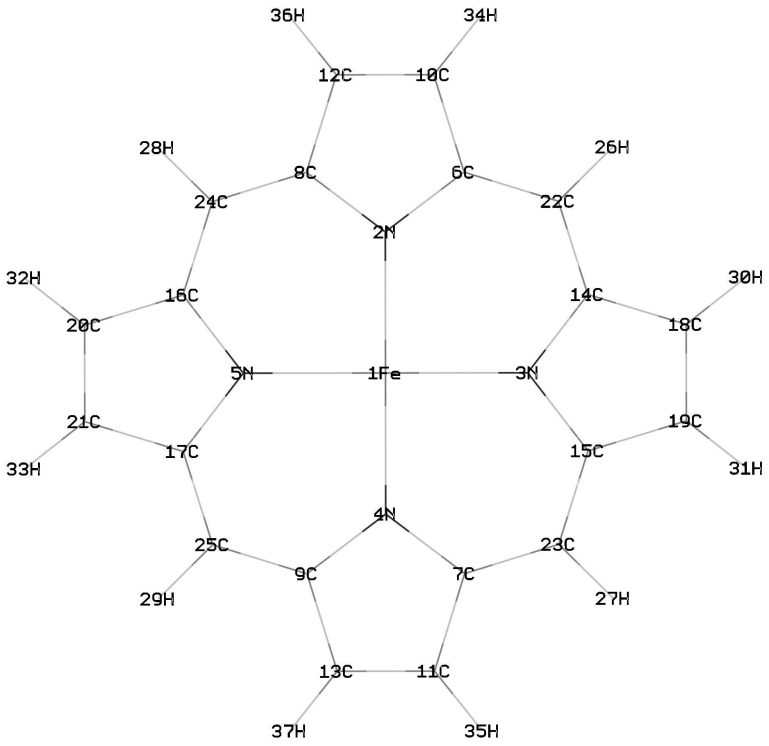

Figure 1.1. Model of FeP molecule. This model is used as a reference diagram for the optimized parameters.

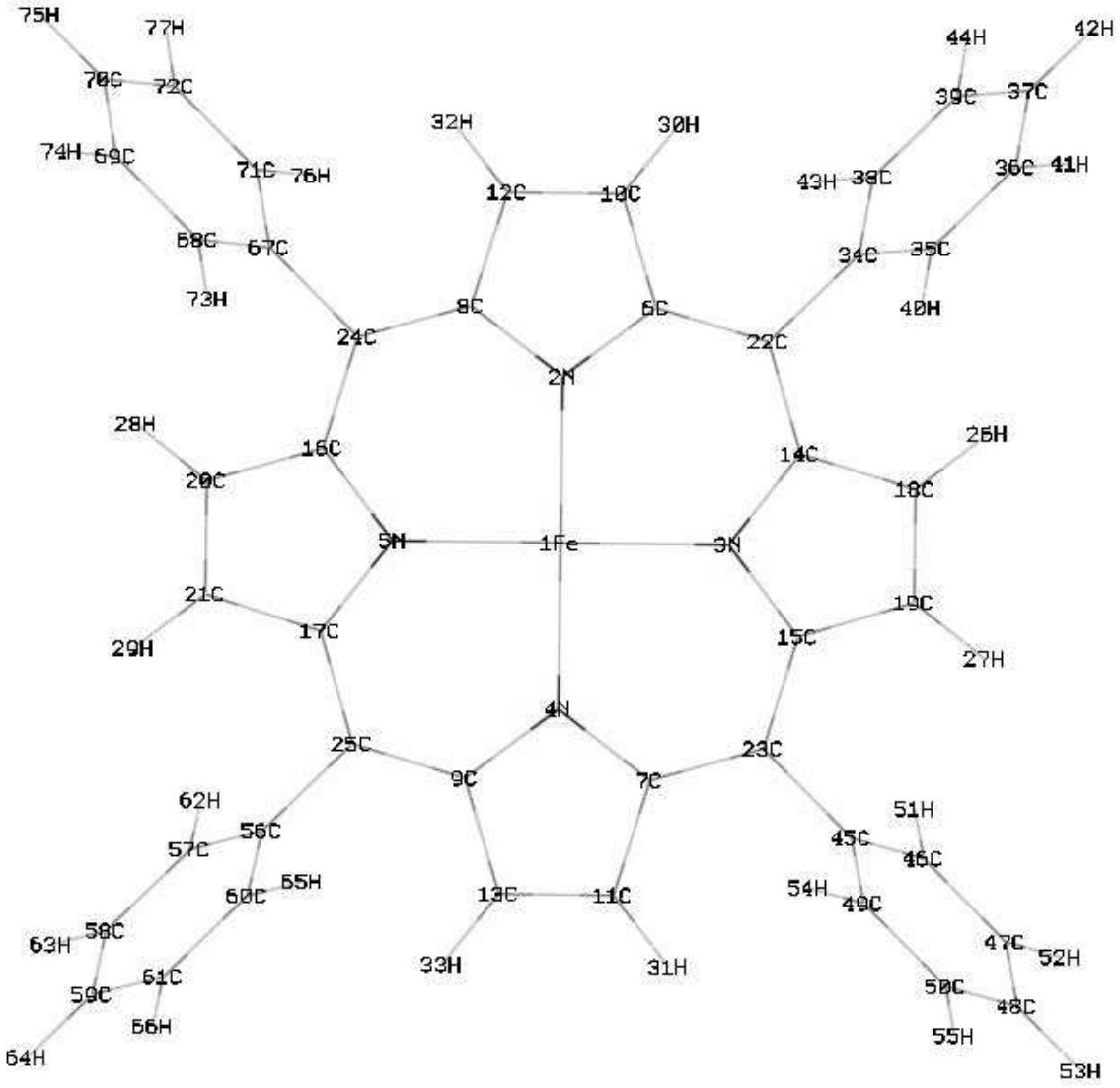

Figure 1.2. Model of FeTPP molecule. This model is used as a reference diagram for the optimized parameters.

Our motivation for studying FeP and FeTPP is to look at iron-tetraphenylporphyrin-sulfonate (FeTPPS) as a photocatalyst in degrading TNT and to determine a possible pathway by which this process occurs within the system of interest. This requires detailed knowledge of the excited states of the system. In light of the aforementioned arguments regarding the actual spin of the ground state and the promising nature of using FeTPPS as a photocatalyst [11], we have studied the S=1 and S=2 iron(II) complexes. Since FeTPPS is a much larger system compared to FeP and only slightly larger than FeTPP, in terms of the number of electrons to account for, we studied the smaller system to interpret the experimental absorption spectrum of FeTPPS. The question to be answered is if we can use the FeP results to understand other properties of FeTPP and FeTPPS. In order to determine this, however, we needed to know the excited state spectra for both spin states of both iron(II) complexes, i.e. FeP and FeTPP.

The next step was to determine how the photocatalyst (FeP) mixed with 2,4,6-trinitrotoluene (TNT) in an aqueous solutions interacts with the system as is discussed by Harmon.[11] It was believed that perhaps electron transfer was the preferred mechanism by which the demethylization of TNT occurred. The final set of products was experimentally determined after this demethylization process by FeTPPS. While the final products are known, the pathway is not yet understood. Therefore, the question remains by what pathway does the process take? While this question may not be one that can be answered in the scope of this work, we can determine whether or not the electron transfer mechanism is a viable process for the system in question.

1.2 Outline of Thesis

The research herein is organized into three main groups. The first group discusses the theoretical aspects of the models employed in this research. The second

group is a discussion of the calculations and gives a comparison of these calculations to observations made experimentally. The third group gives a discussion on the degradation pathway by examining the thermodynamics of the system.

As was mentioned, Chapter 2 introduces the theoretical framework in which the research is built upon. Here a brief introduction to Hartree-Fock Theory (HFT), density functional theory (DFT), and time-dependent density functional theory (TDDFT), and the solvation method will be given. More importantly, a detailed discussion of the density functional used through the calculations will be discussed.

In Chapter 3, the resulting calculations on the system will be given. The system of FeTPP and FeP along with the case of the solvated system of FeP will be included. These calculations of the different multiplets of the systems will be discussed and compared to available experimental data given by other research groups as well as our own.

Chapter 4 and 5 will include the thermodynamic considerations of electron transfer within our system. Results from the calculations will be given and discussed to show the possibility of electron transfer within the molecular systems used in this research. Chapter 6 will then tie everything together as a summary will be given.

CHAPTER 2

THEORY

2.1 Introduction

Different levels of theory can be used for a variety of different applications. For research presented here, HF and DFT were employed to find the lowest energy state termed the ground state. For vertical transition states or electronic excitations, configuration interaction of singles (CIS) and TDDFT were used. As the solvent was included in the system, a method known as the polarizable-continuum model (PCM) was used to model the solvent affects of the molecular system immersed in an aqueous solution.

All the methods above were employed to obtain a comparison of the different levels of theory with each other, i.e. comparing HF to DFT and CIS to TDDFT. In addition to comparing with each other, each set of calculations will be compared to the experimental results that are available. A brief discussion will be given to HF, DFT, and PCM, with a more lengthy explanation on TDDFT and the density functional used in this work involving DFT type calculations.

2.2 Hartree-Fock

The HF method is a model which treats each electron as though it lies in an averaged potential field due to the other $N-1$ electrons. Therefore, the disadvantage of HF is its inability to properly account for electron correlation within the model. In addition, this method calculates the ground state energy as a function of the orbitals

in which the wavefunction is expanded i.e. the basis used. This will be shown to be different from other methods included in this study, mainly the DFT methods.

The model begins with the Hamiltonian consisting of electrons and nuclei of the molecular system as given by Szabo and Ostlund[12] which is

$$H = -\sum_{i=1}^{N} \frac{1}{2}\nabla_i^2 - \sum_{A=1}^{M} \frac{1}{2M_A}\nabla_A^2 - \sum_{i=1}^{N}\sum_{A=1}^{M} \frac{Z_A}{r_{iA}} + \sum_{i=1}^{N}\sum_{i<j}^{N} \frac{1}{r_{ij}} + \sum_{A=1}^{M}\sum_{B=1}^{M} \frac{Z_A Z_B}{R_{AB}}. \quad (2.1)$$

Here N and M are the number of electrons and nuclei respectively. M_A is the mass ratio of nucleus A to the electron, and Z_A represents the atomic number of nucleus A.

Since we are interested in electronic excitations in the scope of this work, we will utilize the electronic Hamiltonian. For this, we utilize the Born-Oppenheimer approximation. This approximation treats the nuclei as stationary relative to the electrons since the nuclei have a greater mass than the electrons. Therefore, the electrons lie within the field of nuclei and the kinetic energy of the nuclei can be neglected. This also leaves the last term in the above equation to be a constant. Taking this approximation into consideration and also the fact that we are interested in electronic energies, the full Hamiltonian can be reduced to give the electronic Hamiltonian H_{elec} as

$$H_{elec} = -\sum_{i=1}^{N} \frac{1}{2}\nabla_i^2 - \sum_{i=1}^{N}\sum_{A=1}^{M} \frac{Z_A}{r_{iA}} + \sum_{i=1}^{N}\sum_{i<j}^{N} \frac{1}{r_{ij}}. \quad (2.2)$$

For simplicity, H_{elec} will now be written as H since the energies we are focusing on will be the electronic energies and not the nuclear energies.

Once this electronic Hamiltonian H is written out, one can employ the use of the HF equations, a set of nonlinear integro-differential equations that must be solved numerically in an iterative fashion. The notation used is that of Szabo and Ostlund.[12] These equations take the form

$$h(1)\chi_a(1) \quad + \quad \sum_{b\neq a}[\int dx_2|\chi_b(2)|^2 r_{12}^{-1}]\chi_a(1)$$
$$- \quad \sum_{b\neq a}[\int dx_2\chi_b^*(2)\chi_a(2)r_{12}^{-1}]\chi_b(b) = \varepsilon_a\chi_a(1) \tag{2.3}$$

with $h(1)$ written as

$$h(1) = -\frac{1}{2}\nabla_1^2 - \sum_A \frac{Z_A}{r_{12}} \tag{2.4}$$

These equations essentially give the best spin orbitals χ that minimize the electronic energy E_0 given as

$$E_0 = \langle\Psi_0|H|\Psi_0\rangle = \sum_a\langle\chi_a|h|\chi_a\rangle + \frac{1}{2}\sum_{ab}\langle\chi_a\chi_b\|\chi_a\chi_b\rangle \tag{2.5}$$

where

$$\langle\chi_a\chi_b||\chi_a\chi_b\rangle = \langle\chi_a\chi_b|r_{12}^{-1}|\chi_a\chi_b\rangle - \langle\chi_a\chi_b|r_{12}^{-1}|\chi_b\chi_a\rangle. \tag{2.6}$$

The total wave function Ψ_0 is that formed by the optimized spin orbitals from the HF equations that minimize the energy E_0. The wave function must be antisymmetic with respect to interchanging two electronic coordinates involving both space and spin. The wave function necessary that includes this property can be obtained from using the a Slater determinant. Therefore the wave function can be written as $\Psi(x_1, x_2, ..., x_N)$ given by

$$\Psi(\mathbf{x}_1, \mathbf{x}_2, \ldots, \mathbf{x}_N) = (N!)^{-1/2}\begin{vmatrix} \chi_i(\mathbf{x}_1) & \chi_j(\mathbf{x}_1) & \ldots & \chi_k(\mathbf{x}_1) \\ \chi_i(\mathbf{x}_2) & \chi_j(\mathbf{x}_2) & \ldots & \chi_k(\mathbf{x}_2) \\ \vdots & \vdots & & \vdots \\ \chi_i(\mathbf{x}_N) & \chi_j(\mathbf{x}_N) & \ldots & \chi_k(\mathbf{x}_N) \end{vmatrix} \tag{2.7}$$

which leads to stating that HF theory (HFT) is a single determinant theory. As can be seen HFT is based on finding the optimum set of orbitals to construct a wave function based on these orbitals i.e. the Slater determinant.

2.2.1 Basis Sets

When performing calculations on molecules one must use the expansion of the MO to mathematically construct the wavefunction of the system. Since the wavefunction is an antisymmeterized product of MOs using a Slater determinant (Eq. 2.7), then it becomes quite a task to computationally arrive at useable data. Therefore, calculations must be performed on computers, and the method used computationally is the basis set approximation. This is the case where the MOs are expanded in terms of a chosen basis, as mentioned earlier in terms of the AOs. Many studies have been done on basis sets such as those by Dunning and Huzinaga, Pople, and many more.[13] However, the former two have gained popularity over other basis sets developed due to extensive calculations done with both basis sets. There is an extensive amount of work in which to compare the level of accuracy within a desired set of calculations.

The basis set used in these proceeding calculations consists of Gaussian Type Orbitals (GTO) since gaussian functions can be integrated analytically, thus allowing for less computational time to be used. There are drawbacks to using GTOs compared to using Slater Type Orbitals (STO). In the limit as the electron-nuclear distance approaches zero there should be a cusp because of the $1/r$ dependence of the coulombic attraction between the nucleus and the electron. Another drawback is the rapid decay of the GTOs at large distances. It is possible to remedy these behavioral problems by using STOs as the basis functions. There is, however, a problem with using STOs as the basis functions. This is due to the large number of multicentered integrals, which take the form

$$\langle \phi_\mu^A \phi_\nu^C | \phi_\lambda^B \phi_\sigma^D \rangle = \int \phi_\mu^{*A}(\mathbf{r}_1) \phi_\nu^{*C}(\mathbf{r}_2) \frac{1}{r_{12}} \phi_\lambda^B(\mathbf{r}_1) \phi_\sigma^D(\mathbf{r}_2). \tag{2.8}$$

This is a multicentered integral, where ϕ_μ^A is a basis function on nucleus A, or centered at $\vec{R}_A$. For an STO 4-centered integral, one would need to evaluate the integral numerically. However, when using a GTO 4-centered integral one can transform these to a 2-centered integral which can then be solved analytically. Thus, one must use an increased number of GTOs to describe a MO, compared to using STOs, to get approximately the same behavior as using STOs. Even though there is an increased number of GTOs used, the time spent evaluating these extra GTOs is considerably less. So computationally speaking, GTOs are a more convenient basis then STOs in which to express the MO.[12]

The types of basis functions used in my analysis are composed of s, p, and d functions. These functions have the following form:

$$\phi_{1s}(\alpha, \mathbf{r}) = (8\alpha^3/\pi^3)^{1/4} e^{-\alpha r^2} \tag{2.9}$$

$$\phi_{2p_x}(\alpha, \mathbf{r}) = (128\alpha^5/\pi^3)^{1/4} x e^{-\alpha r^2} \tag{2.10}$$

$$\phi_{3d_{xy}}(\alpha, \mathbf{r}) = (2048\alpha^7/\pi^3)^{1/4} xy e^{-\alpha r^2} \tag{2.11}$$

with each describing an s, p, and d AO respectively. The α term is the Gaussian orbital exponent. For the s-function there is only one function available since the angular momentum $\ell = 0$. The p-functions have 3 possibilities: p_x, p_y, and p_z (due to $\ell = 1$ giving $m_\ell = -1, 0, 1$) to describe the 3 possible m_ℓ states. For the d-functions there are 5 possible representations: d_{z^2}, $d_{x^2-z^2}$, d_{xy}, d_{yz}, and d_{zx} for the 5 m_ℓ states. Visual representations of these functions have been illustrated in Fig. 2.1[14]

In dealing with basis functions to describe molecular orbitals, it has been found that that the behavior of these basis functions more accurately describes the core electrons and less accurately describes the valence electrons. That is a problem for quantum chemists because most chemical reactions are explained through the interaction of the valence electrons. In response to this problem, a method has been

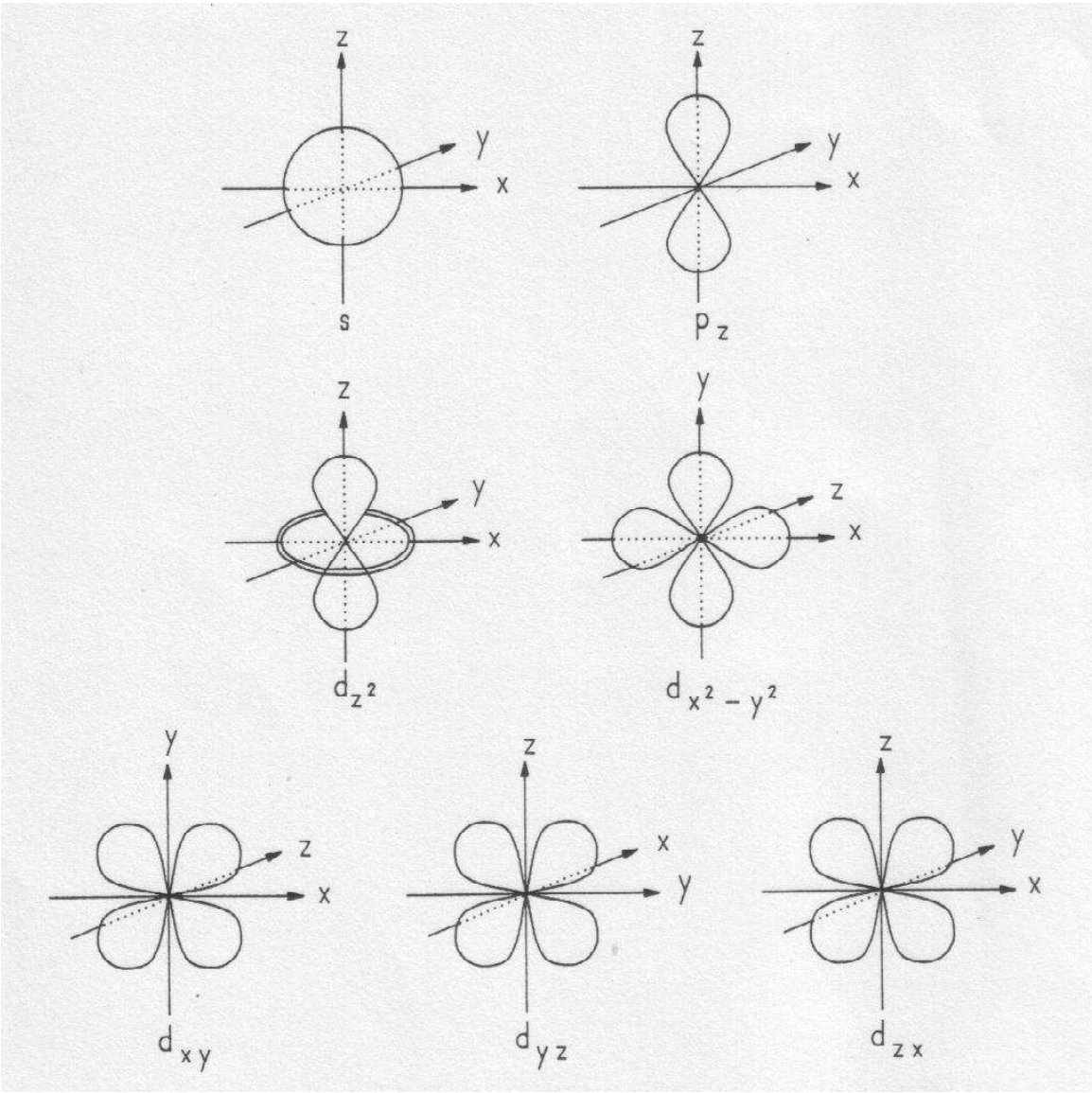

Figure 2.1. Pictographs of the functions used to describe the orbitals.

developed in which the basis sets are contracted to better serve in the calculation of the behavior of these valence electrons. The new basis utilizes what are called contracted Gaussians. These take the form of

$$\phi_{\mu}^{CGF}(\mathbf{r}-\mathbf{R}_A) = \sum_{p=1}^{L} d_{p\mu}\phi_p(\alpha_{p\mu}, \mathbf{r}-\mathbf{R}_A) \tag{2.12}$$

where ϕ_{μ}^{CGF} is the contracted Gaussian basis function, $d_{p\mu}$ are the contraction coefficients, $\alpha_{p\mu}$ are the contraction exponents, and ϕ_p are the primitive Gaussians which make up the contracted Gaussian function. L is the contraction length, or how many contracted primitives there are within a contracted basis function, and are represented by equations 2.9 - 2.11. The method used to define the contraction is more of an art and will not be discussed here.

2.3 Density Functional Theory

Density functional theory is different compared to HFT in that DFT includes within its framework the electron correlation energy. Another difference between HFT and DFT is that DFT is based on the electron density in which all information of the system is extracted through this electron density. As was mentioned in the previous sections HFT is based on extracting the system's information through the wave function.

This method is centered on two theorems known as the Hohenberg-Kohn theorems.[15] The first theorem is stated as "The external potential $v(\mathbf{r})$ is determined, within a trivial additive constant, by the electron density $\rho(\mathbf{r})$."[16] Therefore, in knowing the electron density $\rho(\mathbf{r})$ one can know the electronic properties as well as the wave function if so desired. The second theorem is stated as "For a trial density $\tilde{\rho}(\mathbf{r})$, such that $\tilde{\rho}(\mathbf{r}) \geq 0$ and $\int \tilde{\rho}(\mathbf{r})d\mathbf{r} = N$,

$$E_0 \leq E_v[\tilde{\rho}] \tag{2.13}$$

where $E_v[\tilde{\rho}]$ is the energy functional."[16] The energy functional $E_v[\tilde{\rho}]$ is written as

$$E_v[\tilde{\rho}] = T[\rho] + V_{ne}[\rho] + V_{ee}[\rho] = \int \rho(\mathbf{r}) v(\mathbf{r}) d(\mathbf{r}) + F_{HK}[\rho] \tag{2.14}$$

$$F_{HK}[\rho] = T[\rho] + V_{ee}[\rho] = T[\rho] + J[\rho] + E_{xc}[\rho] \tag{2.15}$$

The term $V_{ee}[\rho]$ includes both classical $J[\rho]$ and non-classical $E_{xc}[\rho]$ energies. It is this non-classical energy that is important for it contains within it the exchange-correlation energy $E_{xc}[\rho]$. We can call this $F_{HK}[\rho]$, or more simply $F[\rho]$, a universal function of $\rho(\mathbf{r})$.

The density which is sought after is the ground state density which minimizes the energy $E[\rho]$. We can now recast this energy of the many electron system as

$$E[\rho] = \int \rho(\mathbf{r}) v(\mathbf{r}) d\mathbf{r} + F[\rho] \tag{2.16}$$

with $F[\rho]$ given above.

The method of calculating the ground state energy as a function of the density is known as the Kohn-Sham method.[17] With this development, the system is initiated by an energy that excludes interacting electrons i.e. a *noninteracting* system. This loss of energy is picked up by the $F[\rho]$ term in the energy expression above. The kinetic energy is also somewhat simplified with the energy difference between the exact energy expression $T[\rho]$ and the approximate expression $T_s[\rho]$ being picked up also by the $F[\rho]$. Now $F[\rho]$ is written as

$$F[\rho] = T_s[\rho] + J[\rho] + E_{xc}[\rho] \tag{2.17}$$

and the total energy expression can be rewritten as

$$E[\rho] = T_s[\rho] + J[\rho] + E_{xc}[\rho] + \int v(\mathbf{r}) \rho(\mathbf{r}) d\mathbf{r} \tag{2.18}$$

Essentially, all the errors due to the approximations made are now contained within the single exchange-energy correlation term $E_{xc}[\rho]$. From the Euler equation comes the effective potential $v_{eff}(\mathbf{r})$ written as

$$v_{eff}(\mathbf{r}) = v(\mathbf{r}) + \frac{\delta J[\rho]}{\delta \rho(\mathbf{r})} + \frac{\delta E_{xc}[\rho]}{\delta \rho(\mathbf{r})} = v(\mathbf{r}) + \int \frac{\rho(\mathbf{r}')}{|\mathbf{r} - \mathbf{r}'|} d\mathbf{r}' + v_{xc}(\mathbf{r}) \tag{2.19}$$

where $v_{xc}(\mathbf{r})$ is known as the exchange-correlation potential. Now the idea is that to improve the total energy $E[\rho]$ all one needs to do is improve the quality of the exchange-correlation potential $v_{xc}(\mathbf{r})$.

The Kohn-Sham development based on this exchange correlation potential and electron density produces a set of equations that allows for one to calculate the ground state in an iterative fashion. These equations adhere to the notation of Parr and Yang[16] which take the form

$$[-\frac{1}{2}\nabla^2 + v_{eff}]\psi_i = \varepsilon_i \psi_i \tag{2.20}$$

$$v_{eff}(r) = v(r) + \int \frac{\rho(\mathbf{r}')}{|\mathbf{r} - \mathbf{r}'|} d\mathbf{r}' + v_{xc}(\mathbf{r}) \tag{2.21}$$

$$\rho(\mathbf{r}) = \sum_{i}^{N} \sum_{s} |\psi_i(\mathbf{r}, s)|^2 \tag{2.22}$$

with the density constrained to the following condition

$$\int \rho(\mathbf{r}) d\mathbf{r} = N \tag{2.23}$$

Once the ground state electron density has been found using the above equations, the total energy of the ground state can be calculated using an expanded expression for the energy $E[\rho]$ given as

$$E[\rho] \quad = \quad \sum_{i}^{N} \langle \psi_i | -\frac{1}{2}\nabla^2 + v_{eff}(\mathbf{r}) | \psi_i \rangle$$

$$- \frac{1}{2}\int \frac{\rho(\mathbf{r})\rho(\mathbf{r}')}{|\mathbf{r}-\mathbf{r}'|}d\mathbf{r}d\mathbf{r}' + E_{xc}[\rho] - \int v_{xc}(\mathbf{r})\rho(\mathbf{r})d\mathbf{r} \tag{2.24}$$

One of the main difference between DFT and HF is that DFT is able to incorporate both the exchange and coulombic correlation effects. Hartree-Fock correctly includes the exchange correlation, but incorrectly includes the coulomb correlation by not including the interaction of electrons with unlike spins. DFT is definitely more advantageous than HF due to DFT having a better scaling factor, with HF scaling as N^4 and DFT scaling as N^3 where N is the number of electrons in the system. With this in mind, it is therefore conceivable that DFT should give a better ground state over HF.

2.4 Time-Dependent Density Functional Theory

Time dependent density functional theory is based on theorems by Runge and Gross.[18] It has been reviewed recently by Marques and Gross[19] in which a detailed discussion is given. I refer the reader to this review article for a detailed explanation of TDDFT. In papers by Stratmann *et al.*[20] and Lourderaj *et al.*[21] TDDFT was applied to molecular systems which is also the case of the research discussed herein. The ideas behind the application of TDDFT to these molecular systems are discussed there and their formulation of the TDDFT equations will be described in this section. The derivation of the equations mainly follows what is given in both Stratmann *et al.* and Lourdera *et al.* We begin by assuming a potential $v_{eff}(\mathbf{r},t)$ for a non-interacting system of particles

$$v_{eff}(\mathbf{r},t) = v(t) + v_{SCF}(\mathbf{r},t) \tag{2.25}$$

$$v_{SCF}(\mathbf{r},t) = \int \frac{\rho(\mathbf{r},t)}{|\mathbf{r}-\mathbf{r}'|}d\mathbf{r}' + v_{xc}(\mathbf{r},t) \tag{2.26}$$

which have the orbitals $\psi(\mathbf{r},t)$ that produce the same charge density $\rho(\mathbf{r},t)$ that the system of interacting particles has. Given this assumption we can write down the time-dependent Kohn-Sham equation

$$[-\frac{1}{2}\nabla^2 + v_{eff}(\mathbf{r},t)]\psi(\mathbf{r},t) = i\frac{\partial}{\partial t}\psi(\mathbf{r},t). \tag{2.27}$$

The exchange potential $v_{xc}(\mathbf{r},t)$ can be written as

$$v_{xc}(\mathbf{r},t) = \frac{\delta A_{xc}[\rho]}{\delta\rho(\mathbf{r})} \tag{2.28}$$

The $A_{xc}[\rho]$ term is the exchange correlation action functional which is over space and time coordinates. This is essentially the time-dependent analogue of the $E_{xc}[\rho]$ in the time-independent system. In making what is known as the adiabatic approximation, which is were the potential varies slowly with time, the exchange-correlation potential can be approximated by

$$v_{xc}(\mathbf{r},t) = \frac{\delta E_{xc}[\rho_t]}{\delta\rho_t(\mathbf{r})} = v_{xc}[\rho_t](\mathbf{r}) \tag{2.29}$$

where the potential $v_{xc}[\rho_t]$ varies over space at some fixed time t.

As the system is in its ground state, a perturbation is introduced into the system by an applied field $\delta v(t)$ to first order giving

$$\delta v_{eff}(\mathbf{r},t) = \delta v(t) + \delta v_{SCF}(\mathbf{r},t). \tag{2.30}$$

The $\delta v_{SCF}(\mathbf{r},t)$ term is the linear response in the self-consistent field due to the change in the charge density. This charge density is given in a frequency representation and is written as

$$\delta\rho(\mathbf{r},\omega) = \sum_{lm}\delta P_{lm}(\omega)\psi_l(\mathbf{r})\psi_m^*(\mathbf{r}) \tag{2.31}$$

where the δP_{lm} is the Kohn-Sham density matrix in the basis of unperturbed orbitals.

A new expression can be obtained for this density matrix if the density is divided into two parts–the hole-particle (δP_{ia}) and particle-hole (δP_{ai}) parts. With this new expression $\delta\rho(\mathbf{r},\omega)$ becomes

$$\delta\rho(\mathbf{r},\omega) = \sum_{lm} \delta P_{ai}(\omega)\psi_a(\mathbf{r})\psi_i^*(\mathbf{r}) + \sum_{lm} \delta P_{ia}(\omega)\psi_i(\mathbf{r})\psi_a^*(\mathbf{r}) \tag{2.32}$$

where i, j and a, b represent the occupied and unoccupied orbitals. The indices of l, m, u, and v will represent dummy indices of general orbitals.

Using perturbation theory, we can write the response of the Kohn-Sham density matrix to the applied field. This gives

$$\delta P_{lm}(\omega) = \frac{\Delta n_{lm}}{(\epsilon_l - \epsilon_m - \omega)} \delta v_{lm}^{eff}(\omega) \tag{2.33}$$

with Δn_{lm} being the difference in occupation numbers. $\Delta n_{lm} = 1$ for $lm = ai$ and $\Delta n_{lm} = -1$ for $lm = ia$. We can describe the linear response of the self-consistent field to the change in the charge density by defining a coupling matrix $K_{lm,uv}$ written as

$$\begin{aligned} K_{lm,uv} &= \frac{\partial v_{lm}^{SCF}}{\partial P_{uv}} = \int\int \psi_l^*(\mathbf{r})\psi_m(\mathbf{r}) \frac{1}{|\mathbf{r}-\mathbf{r'}|} \psi_v(\mathbf{r'})\psi_u^*(\mathbf{r}) d\mathbf{r} d\mathbf{r'} \\ &+ \int\int \psi_l^*(\mathbf{r})\psi_m(\mathbf{r}) \frac{\delta^2 E_{xc}}{|\delta\rho(\mathbf{r}) - \delta\rho(\mathbf{r'})|} \psi_v(\mathbf{r'})\psi_u^*(\mathbf{r}) d\mathbf{r} d\mathbf{r'}. \end{aligned} \tag{2.34}$$

The derivative above is taken with respect to the ground state density. Noting that the coupling matrix $\mathbf{K}$ has both the coulombic and exchange-correlation the potential v_{SCF} in δv_{lm}^{eff} can be expressed in terms of the coupling matrix and is given as

$$\delta v_{lm}^{SCF}(\omega) = \sum_{bj} K_{lm,bj}(\omega)\delta P_{bj}(\omega) + \sum_{jb} K_{lm,jb}(\omega)\delta P_{jb}(\omega). \tag{2.35}$$

Given the above equations we are now in a position to calculate δP_{lm} and δv_{lm}^{SCF} self-consistently, as they depend on the the linear response of the density matrix. Putting

together the expressions for $v_{eff}(\mathbf{r},t)$, $\delta P_{st}(\omega)$, and $\delta v_{st}^{SCF}(\omega)$ with some algebra, we have the coupled matrix equations given as

$$\begin{pmatrix} \mathbf{A} & \mathbf{B} \\ \mathbf{B}^* & \mathbf{A}^* \end{pmatrix} \begin{pmatrix} \mathbf{X} \\ \mathbf{Y} \end{pmatrix} = \omega \begin{pmatrix} 1 & 0 \\ 0 & -1 \end{pmatrix} \begin{pmatrix} \mathbf{X} \\ \mathbf{Y} \end{pmatrix} \tag{2.36}$$

Here matrices $\mathbf{A}$, $\mathbf{B}$, $\mathbf{X}$, and $\mathbf{Y}$ are give as

$$A_{ai,bj} = \delta_{ab}\delta_{if}(\epsilon_a - \epsilon_i) + K_{ai,bj} \tag{2.37}$$

$$B_{ai,bj} = K_{ai,jb} \tag{2.38}$$

$$X_{ai} = \delta P_{ai}(\omega) \tag{2.39}$$

$$Y_{ai} = \delta P_{ia}(\omega) \tag{2.40}$$

The electronic excitations are then given by the poles of $\delta P_{lm}(\omega)$, and can also be calculated by finding the eigenvalues ω from the matrix equation above.

2.5 Configuration Interaction

Time-dependent density functional theory is only one of a few ways in which to calculated the vertical electronic excitation spectrum. In our work presented here we also employed the method of CIS. In this method the wave function of the system is composed of multiple excited determinants. So the exact wave function for any state takes the form

$$|\Phi\rangle = c_0|\Psi_0\rangle + \sum_{ra} c_a^r|\Psi_a^r + \sum_{r<b,r<s} c_{ab}^{rs}|\Psi_{ab}^{rs} + \dots . \tag{2.41}$$

The CIS method makes use of only the ground state and singly excited determinants, i.e. $|\Psi_0\rangle$ and $\sum_{ra} c_a^r |\Psi_a^r$. With the excitation energies calculated using only singly excited determinants, there is no inclusion of correlation energy.

With an increased number of excited determinants used, a better ground state energy and electronic excitation are calculated as it includes a better result due to the inclusion of the correlation energy. That is to say including the doubly, triply, etc. excited state determinants, the energies calculated become closer to the actual ground state due to higher order correlation effects. What makes this method not as advantageous as TDDFT is the fact that the higher order correlation effects become very expensive computationally compared to TDDFT.

2.6 Polarizable-Continuum Model

Most, if not all, chemical reactions which are investigated involve some type of solvent. Therefore, it stands to reason that the equations that are used to predict the electronic transitions should be modified to include the solvent-solute interaction of the system of interest. A model which takes this interaction into account is that of the Polarizable-Continuum Model (PCM). Cossi and Barone[22] develop the necessary modifications to TTDFT to include solvent-solute interactions into the electronic transitions. In this model, the molecules in the solvent system are treated quantum mechanically, while the solvent is treated as a continuum.

"The physical picture underlying the PCM is based on a sharp partition between the solute (one or more molecules, described at the desired level of theory) and the solvent, represented as a structureless infinite continuum, characterized by its macroscopic dielectric constant and density."[22] This boundary is closed, and is built by a spherical surface around the solute molecule. Inside the sphere containing the solute the dielectric is 1 which is to represent that of a vacuum. Just outside the cavity enclosing the solute the dielectric becomes that of the solvent used. For

instance if water is used as the solvent, as is the case in our study, the dielectric of 80.2 is used outside the sphere.

To account for the shape of the molecule, the cavity is generated by a number of overlapping spheres about the atoms of the molecule. The formation of the cavity and implementation is derived by Pascual-Ahuir *et. al.*.[23] The radii of the spheres used have been optimized by Barone *et. al.*[24] to give values of the solvation free energies of various molecules which agree with experimental values. Cossi and Barone[22] implement their formulation of PCM in TDDFT in pyridazine, and pyrimidine in different solvents. The authors show the calculated electronic excitations are in fairly good agreement with experimental values.

CHAPTER 3

CALCULATIONS

3.1 Introduction

In this chapter, the results from the TDDFT and CIS calculations for the unsolvated and solvatetd complexes will be given for the different multiplets of FeP. For the FeTPP case, only the TDDFT results will be given, for the CIS method was not used for this iron complex. For the solvated system, only the FeP complexes implementing the TDDFT will be given for the different multiplets.

In previous works regarding the structure of four-coordinated FeP, two different symmetries have been used. Most researchers have used a symmetry of D_{4h} to model the geometry of the molecule [2,5–8,10]. Other researchers have used a less constrictive geometry of D_{2h} [25]. In the work presented here, we used the D_{2h} symmetry group in an attempt to give the geometry more freedom to adjust during optimization while still taking advantage of the high symmetry for computational convenience. Similar optimizations were done by Matsuzawa *et al.* [26] employing the D_{2h} symmetry group.

According to Kozlowski *et al.* [4] there are four possible electronic configurations within the D_{4h} symmetry group. Through data obtained by Mössbauer spectra [27] and magnetic data [8] on FeTPP, the accepted ground state is that of the ${}^3A_{2g}$ configuration. This same configuration has also been proposed by Goff *et al.* [10] from NMR spectra from the spatial symmetry. From our results of the D_{2h} symmetry group, we obtained a configuration of ${}^3B_{3g}(d_{xz}, d_{yz})_\alpha(d_{xy}, d_{z^2})^2$ which corresponds to a ${}^3A_{2g}(d_{xz}, d_{yz})_\alpha(d_{xy}, d_{z^2})^2$ after transforming to the D_{4h} symmetry group with the z-axis perpendicular to the plane of the molecule. For the quintet, we obtained a

configuration of ${}^5A_g(d_{xz}, d_{xy}, d_{yz}, d_{y^2-x^2})_\alpha(d_{z^2})^2$ for the D_{2h} symmetry group, which corresponds to the same configuration in the D_{4h} symmetry group with the z-axis perpendicular to the plane of the FeP molecule.

In earlier studies dealing with the four-coordinated FeTPP, some groups have used an S_4 symmetry group, or quasi-D_{2h}, which is a ruffling of the porphyrin core and displacement of the iron atom from the center of the four nitrogen bonds within the center of the molecule [8,28,29]. The use of the symmetry is due to the findings of X-ray analysis of the structure. In our model of FeTPP, we employed the use of D_{2h} before optimization of the molecule. Further optimization of FeTPP gave a C_{2v} symmetry for the ground state due to the "saddle" distortion of the main molecule with the nitrogen atoms sticking out of the plane and the rotation of the phenyl rings approximately 47° from the plane of the core macrocycle.

All calculations included in this analysis were initially started using unrestricted HF employing the basis set 6-31G(d,p) for all the atoms. This was done to get a starting point for the orbitals. Further optimizations were then carried out using Kohn-Sham DFT [16] and the B3LPY [30] exchange-correlation density functional. The excited states for the FeP were calculated using both CIS and TDDFT, while TDDFT was the only method used for determining the excited states of FeTPP. All TDDFT calculations were approached using the adiabatic approximation as described by Stratmann *et al.* [20]. A comparison of CPU times for FeP and FeTPP could not be made since calculations were done on different computer clusters. For FeP 456 basis functions were used, and for FeTPP 896 basis functions were used.

3.2 Unsolvated FeP and FeTPP Complexes

3.2.1 Geometry Optimization FeP

We determined the optimized geometry for each of the S=0, 1, and 2 spin states. For the optimizations we used the density functional B3LYP, and constrained

	S=1	S=2	S=0
	Energy (au)	Energy (au)	Energy (au)
FeP	-2252.098	-2252.091	-2252.034
FeTPP	-3176.326	-3176.317	-3176.259

TABLE 3.1. Tabulated are the optimized FeP and FeTPP total energies of the different spin states.

the symmetry to D_{2h}. For all three spin states, the iron atom was not displaced from the center. Table 3.1 shows the total energy of these different spin states for FeP and FeTPP. Rovira *et al.* [6] performed a similar study of geometrically optimizing each spin state independently; however, they artificially displaced the iron atom $0.3\mathring{A}$ out of plane and allowed it to relax into the plane. This relaxation produced a molecular geometry having the iron atom displaced from the plane by $0.08\mathring{A}$. No displacement of the iron atom from the molecule's center was observed in the results of our calculations. This is possibly due to finding a local minimum within the geometry optimization process. In looking at this same issue, Kozlowski *et al.* [4] also report no displacement of the iron atom from the center.

The optimized geometries obtained from our calculations for the unsolvated FeP mulitplets are given in Table 3.2 and 3.3. In comparing the geometries of the different spin states we can see a subtle difference in the bond lengths and bond angles between the singlet and triplet. However, a more pronounced difference exists for some of the parameters for the quintet compared to the other two multiplets. This is illustrated in Tables 3.2 and 3.3 where the values refer to Figure 1.1. The bond length in the quintet is longer than in the triplet, and the triplet is slightly longer than the singlet. One might attribute this to the spin-spatial dependency arguing that the higher the spin multiplicity, the greater the spatial occupation or spatial extension. However, a recent theoretical study suggests this is not the case. Ugalde *et al.* [31] state that with

Bond Length	Singlet (Å)	Triplet (Å)	Quintet (Å)	Exp* (Å)
Fe - N2	1.996	1.998	2.056	1.972
Fe - N3	1.996	1.997	2.056	1.972
Fe - N4	1.996	1.998	2.056	1.972
Fe - N5	1.996	1.997	2.056	1.972
N2 - C6	1.394	1.393	1.374	1.379
C6 - C10	1.444	1.445	1.445	1.431
C10 - C12	1.366	1.366	1.364	1.353
C6 - C22	1.385	1.386	1.398	1.389
N3 - C14	1.394	1.393	1.374	1.379
C14 - C18	1.444	1.445	1.445	1.431
C18 - C19	1.366	1.366	1.364	1.353
C14 - C22	1.385	1.386	1.398	1.389
C8 - C12	1.444	1.446	1.445	1.440
C15 - C19	1.444	1.446	1.445	1.440
N2 - C8	1.394	1.393	1.374	1.384
N3 - C15	1.394	1.393	1.374	1.384
C8 - C24	1.385	1.386	1.398	1.395
C15 - C23	1.385	1.386	1.398	1.395

TABLE 3.2. Tabulated are the FeP bond lengths of the different spin states. *These values are taken from FeTPP from reference 8.

Bond Angle	Singlet (deg)	Triplet (deg)	Quintet (deg)	Exp* (deg)
N3 - Fe - N4	90.0	90.0	90.0	90.01
Fe - N3 - C14	127.4	126.5	126.5	127.1
N3 - C14 - C22	125.3	125.1	125.1	125.2
C14 - C22 - C6	124.7	126.9	126.9	123.5
Fe - N3 - C15	127.4	126.5	126.5	127.4
N3 - C15 - C23	125.3	125.1	125.1	125.0
C19 - C15 - C23	124.4	125.4	125.4	124.5
N3 - C14 - C18	110.3	109.5	109.5	110.0
C14 - C18 - C19	107.1	107.0	107.0	106.9
C18 - C19 - C15	107.1	107.0	107.0	107.3
N3 - C15 - C19	110.3	109.5	109.5	110.3
C14 - N3 - C15	105.2	107.0	107.0	105.4

TABLE 3.3. Tabulated are the FeP bond angles of the different spin states. *These values are taken from FeTPP from reference 8.

increasing multiplicity of the FeP there is a decrease in atomic radius, thus decreasing the spatial occupation of the atom. No attempt was made in this study to resolve the apparent disagreement.

Tables 3.2 and 3.3 also give the experimental results of FeTPP from X-ray data. As can be seen, the three different spin states of FeP agree reasonably well with the experimental findings for both the bond lengths and bond angles.

3.2.2 Geometry Optimization FeTPP

The same density functional used to optimize the structure of FeP was also used with FeTPP, which was the B3LYP. Table 3.1 gives the total energies of FeTPP as well. It is worth noting that for each spin state the energy difference between that spin state and the ground state is very similar for both FeP and FeTPP. For instance, the difference in energy between the triplet and quintet of FeP is 0.20eV and FeTPP is 0.25eV. The difference between the triplet and the singlet is 1.74eV for FeP and 1.82eV for FeTPP. Therefore we see a similar ordering of the multiplets with similar energy differences.

As with the FeP system, we compare the triplet and quintet states of the FeTPP system. The parameters given are those of the marcocycle common in FeP and FeTPP and the phenyl rings of FeTPP. Figure 1.2 shows the geometric setup in which the bond lengths and bond angles are referenced in Table 3.4 and 3.5. The bond lengths and bond angles for both the triplet and quintet are very close in magnitude with the quintet bond lengths being slightly larger in almost every bond. There is consistent deviation from the experimental values for the theoretical results within the phenyl ring. Overall, however, our calculated results are in very good agreement with the experimental findings.

Bond Length	Triplet (Å)	Quintet (Å)	Exp* (Å)
Macrocycle			
Fe - N2	1.993	2.057	1.972
Fe - N3	1.993	2.057	1.972
N2 - C6	1.383	1.377	1.379
C6 - C10	1.439	1.444	1.431
C10 - C12	1.358	1.362	1.353
C6 - C22	1.397	1.409	1.389
N3 - C14	1.383	1.377	1.379
C14 - C18	1.439	1.444	1.431
C18 - C19	1.358	1.362	1.353
C14 - C22	1.397	1.409	1.389
C8 - C12	1.439	1.444	1.440
C15 - C19	1.439	1.444	1.440
N2 - C8	1.383	1.377	1.384
N3 - C15	1.383	1.377	1.384
C8 - C24	1.397	1.409	1.395
C15 - C23	1.397	1.409	1.395
Phenyl Ring			
C34 - C35	1.404	1.404	1.383
C35 - C36	1.395	1.395	1.394
C36 - C37	1.396	1.396	1.358
C37 - C39	1.396	1.396	1.367
C39 - C38	1.395	1.395	1.402
C34 - C38	1.404	1.404	1.374
C22 - C34	1.497	1.498	1.509

TABLE 3.4. Tabulated are the FeTPP bond lengths of the triplet and quintet spin states. *These values are taken from FeTPP from reference 8.

Bond Angle	Triplet (deg)	Quintet (deg)	Exp* (deg)
Macrocycle			
N3 - Fe - N4	90.0	90.0	90.01
Fe - N3 - C14	127.4	126.4	127.1
N3 - C14 - C22	126.0	125.9	125.2
C14 - C22 - C6	122.9	125.1	123.5
Fe - N3 - C15	127.4	126.4	127.4
N3 - C15 - C23	126.0	125.9	125.0
C19 - C15 - C23	123.5	124.7	124.5
N3 - C14 - C18	110.6	109.4	110.0
C14 - C18 - C19	106.9	107.1	106.9
C18 - C19 - C15	106.9	107.1	107.3
N3 - C15 - C19	110.6	109.4	110.3
C14 - N3 - C15	105.1	106.9	105.4
Phenyl Ring			
C22 - C34 - C35	120.7	120.8	121.1
C22 - C34 - C38	120.7	120.8	119.7
C34 - C35 - C36	120.7	118.4	119.5
C35 - C36 - C37	120.2	120.2	120.4
C36 - C37 - C39	119.6	119.6	120.7
C37 - C39 - C38	120.2	120.2	119.3
C39 - C38 - C34	120.7	120.8	120.5
C35 - C34 - C38	118.5	118.4	119.2

TABLE 3.5. Tabulated are the FeTPP bond angles of the triplet and quintet spin states. *These values are taken from FeTPP from reference 8.

3.3 Unsolvated Excited States of FeP and FeTPP

3.3.1 Unsolvated FeP Excited States

We calculated the excited states and oscillator strengths of the FeP molecule using two different levels of theory. Both CIS and TDDFT were used to obtain these excited states. In Tables 3.6 and 3.7 for the S=1 state, and Tables 3.8 and 3.9 for the S=2 state, we show the first few excited states obtained using both methods for the FeP system respectively. In Table 3.10 we show only the S=0 excitations

Comparing the two TDDFT excitation spectra of the triplet and quintet, one observes a very close correspondence between the electric dipole allowed transitions. We believe this correspondence between the electric dipole allowed transitions is significant in that for the experimental absorption spectrum in Figure 3.1, one cannot be certain if the FeTPPS in aqueous solution is in the S=1 or the S=2 state. These similarities can be seen by looking at the transition states. We noticed a 616nm peak in the triplet excitation spectrum and a 618nm peak in the quintet excitation spectrum – a very close correspondence. Again, in the triplet we see a 518nm peak and a 523nm peak in the quintet giving a close correspondence with the 566nm peak. Going down the list of data, we can see a similar trend in the excitation values of the two systems.

In comparing the CIS excitation spectrum of the triplet and quintet, we see a similar trend between the two systems as was seen within the TDDFT framework. For instance, in the triplet there is a weak 869nm peak, which has a corresponding peak of 857nm in the quintet system. The trend continues through the electric dipole allowed excitations. However, the difference in the corresponding peak values is greater in the CIS comparison than in the TDDFT comparison, which is likely due to the neglect of correlation and other approximations in the CIS approach.

Figure 3.1 shows an experimental absorption spectrum of iron(II)-tetraphenylporphyrin-sulfonate (FeTPPS) in pH 7 buffer.[32] The absorbance spectra of FeTPPS

Final Symm State	Excitation Energy (eV) Calculated	Excitation Wavelength (nm) Calculated	Oscillator Strength Calculated
$1B_{1g}$	0.4410	2811.37	0
$1B_{2g}$	0.4412	2810.14	0
$1B_{2u}$	1.7330	715.45	0.0003
$1B_{1u}$	1.7330	715.44	0.0003
$2B_{1u}$	2.0099	616.87	0.0028
$2B_{2u}$	2.0100	616.85	0.0028
$3B_{2u}$	2.3929	518.14	0.0016
$3B_{1u}$	2.3929	518.13	0.0017
$4B_{2u}$	3.1916	388.47	0.0028
$4B_{1u}$	3.1922	388.40	0.0029
$5B_{2u}$	3.3608	368.91	0.6464
$5B_{1u}$	3.3608	368.91	0.6466

TABLE 3.6. TDDFT calculated excitation results for the FeP S=1 ($^3B_{3g}$) state.

Final Symm State	Excitation Energy (eV) Calculated	Excitation Wavelength (nm) Calculated	Oscillator Strength Calculated
$1B_{1g}$	0.2772	4473.30	0
$1B_{2g}$	0.2772	4471.69	0
$1B_{1u}$	1.4259	869.63	0.0039
$1B_{2u}$	1.4263	869.38	0.0039
$2B_{2u}$	2.2803	543.79	0.0098
$2B_{1u}$	2.2804	543.76	0.0098
$3B_{1u}$	2.5776	481.07	0.0403
$3B_{2u}$	2.5777	481.05	0.0402
$4B_{2u}$	3.8022	326.20	0.0041
$4B_{1u}$	3.8022	326.13	0.0041
$5B_{2u}$	4.7294	262.19	2.5540
$5B_{1u}$	4.7296	262.18	2.5541

TABLE 3.7. CIS calculated excitation results for the FeP S=1 ($^3B_{3g}$) state.

Final Symm State	Excitation Energy (eV) Calculated	Excitation Wavelength (nm) Calculated	Oscillator Strength Calculated
$1B_{3g}$	0.4123	3007.00	0
$1B_{1g}$	0.6083	2038.26	0
$1B_{2g}$	0.6083	2038.17	0
$1B_{2u}$	1.6814	737.40	$< 10^{-4}$
$1B_{1u}$	1.6815	737.36	$< 10^{-4}$
$2B_{1u}$	2.0044	618.57	0.0016
$2B_{2u}$	2.0045	618.52	0.0016
$3B_{2u}$	2.3630	524.68	0.0003
$3B_{1u}$	2.3631	524.67	0.0003
$4B_{2u}$	3.1974	387.76	0.0001
$4B_{1u}$	3.1979	387.71	0.0001
$5B_{2u}$	3.3564	369.39	0.6682
$5B_{1u}$	3.3565	369.38	0.6684
$6B_{2u}$	3.6943	335.61	0.0346
$6B_{1u}$	3.6945	335.59	0.0347

TABLE 3.8. TDDFT calculated excitation results for the FeP S=2 (^5A_g) state.

Final Symm State	Excitation Energy (eV) Calculated	Excitation Wavelength (nm) Calculated	Oscillator Strength Calculated
$1B_{2g}$	0.4736	2618.24	0
$1B_{1g}$	0.4737	2617.69	0
$1B_{3g}$	0.5142	2411.51	0
$1B_{1u}$	1.4453	857.95	0.0010
$1B_{2u}$	1.4455	857.83	0.0010
$2B_{2u}$	2.2621	548.16	0.0030
$2B_{1u}$	2.2622	548.14	0.0031
$3B_{1u}$	2.5175	492.55	0.0357
$3B_{2u}$	2.5175	492.55	0.0356
$4B_{2u}$	3.7568	330.07	0.0002
$4B_{1u}$	3.7572	330.03	0.0002
$5B_{2u}$	4.7021	263.71	2.5909
$5B_{1u}$	4.7023	263.70	2.5916
$6B_{1u}$	5.2030	238.32	0.0022
$6B_{2u}$	5.2031	238.32	0.0022

TABLE 3.9. CIS calculated excitation results for the FeP S=2 (^5A_g) state.

Final Symm State	Excitation Energy (eV) Calculated	Excitation Wavelength (nm) Calculated	Oscillator Strength Calculated
$1B_{2u}$	1.8851	657.52	0.0121
$1B_{3u}$	2.0262	611.91	0.0304
$2B_{2u}$	2.6852	461.73	0.0474
$2B_{3u}$	2.7942	443.72	0.0155
$3B_{2u}$	3.1618	392.13	0.0004
$4B_{2u}$	3.4545	358.90	0.1646
$3B_{3u}$	3.5831	346.02	0.7163
$5B_{2u}$	3.7389	331.60	0.0293
$4B_{3u}$	3.9124	316.90	0.0384
$6B_{2u}$	4.0475	306.32	0.6997
$5B_{3u}$	4.3439	285.42	0.0886
$7B_{2u}$	4.3685	283.82	0.3712

TABLE 3.10. TDDFT calculated excitation results for the FeP S=0 (^1A_g) state.

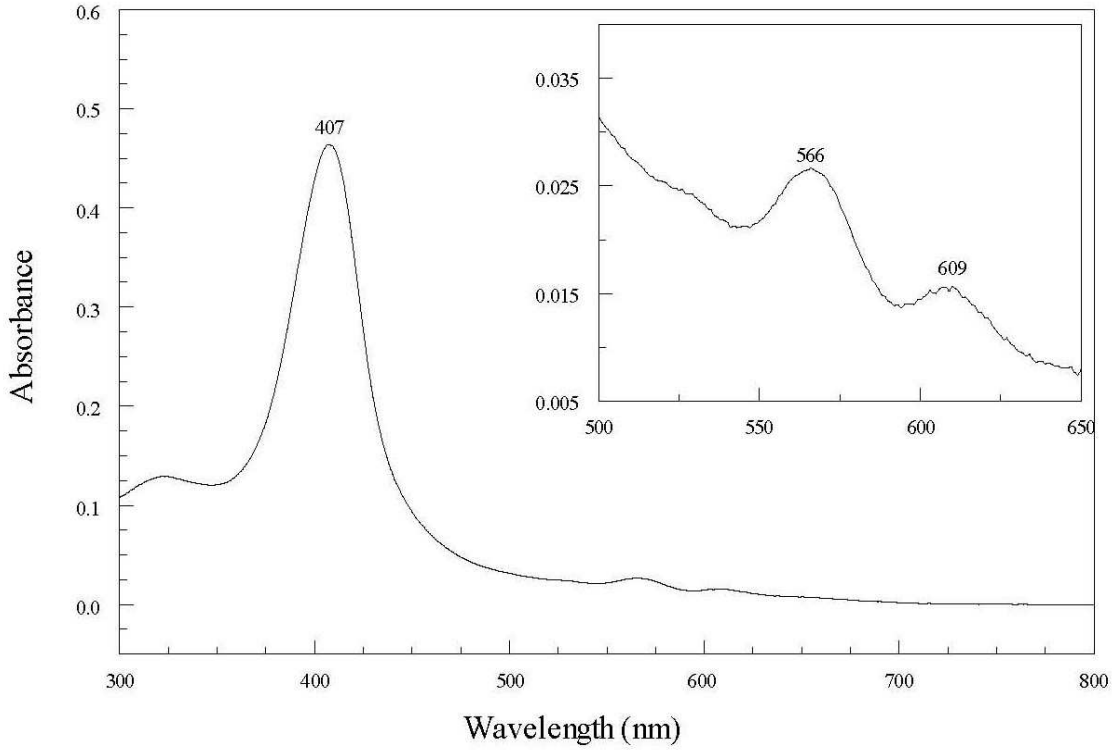

Figure 3.1. Absorbance spectrum of 6.7 μM FeTPPS in pH 7 buffer. Inset are the Q-bands of FeTPPS.

(Frontier Scientific Inc., Logan UT; used without further purification) was resolved by a CARY 4000 UV-Vis spectrophotometer (Varian Instruments). We compare the theoretical excitation spectrum of FeP calculated using TDDFT and CIS with this spectrum. FeTPPS is slightly different from FeTPP and more so from FeP due to the phenylsulfonate groups. However, the sulfonate groups only serve to make the FeTPP soluble in water and have little or no effect on the absorption spectrum for the FeTPP.[33] In Figure 3.1 the largest peak can been seen at 407nm with small peaks at 566nm and 609nm. In the TDDFT theoretical absorption spectrum for the S=1 case of FeP we have an excitation peak at 368nm and 388nm which we believe corresponds to the 407nm Soret band of the absorption spectrum. The large oscillator strength at 368nm is strong evidence of this correspondence between the theoretical spectrum and experimental spectrum. The other absorption peaks appearing in Figure 3.1, i.e. at 566nm and 609nm, correspond to peaks in the theoretical excitation spectrum at 518nm and 616nm respectively. The theoretical peak at 715nm has a relatively weak oscillator strength and is not observed in the experimental spectrum.

Kobayashi and Yanagawa [34] have published an experimental spectrum of FeTPP in benzene. Their spectrum shows a double peak structure (see figure 3 on page 452 in reference 32). Reverse saturable absorption (RSA) has been reported in the tetraphenylporphyrins, including H_2TPP, CoTPP, and ZnTPP [35] and in FeTPP [36]. In the cases of H_2TPP, CoTPP, and ZnTPP, the RSA is associated with an intersystem crossing from the singlet excited state to the ground state of the triplet spin system. In the case of Fe(II)TPP, our results suggest it occurs between the triplet and quintuplet spin systems. The decay from the ${}^5A_g$ ground state of the S=2 spin system to the ${}^3B_{3g}$ ground state of the FeTPP is both symmetry and spin forbidden. Thus, the excitation of FeTPP will result in intersystem crossing and a build up of population in the S=2 system. This results in the simultaneous excitations of both spin systems appearing in both of the experimental absorption spectra. From the excitation energies listed in Tables 3.6 and 3.8 for the S=1 and S=2 spin systems of FeP, we calculated the

λ(Exp,nm)[a]	E(Exp,eV)	ΔE(Exp,eV)	λ(Calc,nm)	E(Calc,eV)	ΔE(Calc,eV)
816.33	1.5190	0.0852	737.4, S=2	1.68	0.051
772.95	1.6042		715.45, S=1	1.7333	
698.69	1.7747	0.0620	616.95, S=1	2.0099	0.0055
675.11	1.8367		618.64, S=2	2.0044	
544.22	2.2785	0	524.76, S=2	2.3630	0.0299
-	-		518.20, S=1	2.3929	
444.44	2.7900	0.1627	369.39, S=2	3.3564	0.0044
419.95	2.9527		368.91, S=1	3.3608	

TABLE 3.11. Comparison of the calculated TDDFT excited states of Fe.
[a] Values taken from Kobayashi and Yanagawa.[34]

projected energy difference between the two sets of peaks and compared these with those of Kobayashi and Yanagawa [34]. These are given in Table 3.11.

This is unlike the situation in H_2TPP, CoTPP, and ZnTPP, where the intersystem crossing occurs from the excited singlet state to the triplet ground state; we see no evidence for a triplet-singlet intersystem crossing in FeTPP. The singlet excitation energies given in Table 3.10 do not agree with the Harmon and Rahaman[32] spectrum (Figure 3.1) or that of Koybashi and Yanagawa [34].

For the first set of absorption peaks our calculated results are similar, however, the calculated oscillator strengths are relatively weak. The energy difference between the peaks theoretically is close to that experimentally. For the remaining peaks we see a similar peak structure with similar energy differences. The experimental peak at 544nm does not seem to show a double peak in that region. However, given the width of the peak, it is possible the two peaks are too close together to be observed individually. Our calculations for the S=1 and S=2 systems predict a double peak structure.

3.3.2 Unsolvated FeTPP Excited States

The excitation spectrum of FeTPP as determined from the TDDFT results gives a spectrum similar to that of FeP. The calculated results can also be compared more directly to the experimental spectra of FeTPPS and FeTPP as was done for the FeP system. Tables 3.12 and 3.13 contain the calculated theoretical dipole allowed transitions for the triplet and quintet systems of FeTPP.

The results show a some close correspondence between the triplet and quintet states of FeTPP. The small oscillator strengths associated with the $5(B_1,B_2)$ and $6(B_1,B_2)$ excitations of the triplet state and the $5(B_2,B_1)$ excitations of the quintet state accounts for their negligible contribution to the absorption spectra. Note that for the $9(B_1,B_2)$ and $10(B_2,B_1)$ excitations of the quintet state, we do not show a corresponding excitation in the triplet state because we didn't compute enough excitation states for the triplet calculations.

Comparison of the experimental absorption spectrum of FeTPPS in Figure 3.1 to the theoretical excitation spectra in Tables 3.12 and 3.13 show a reasonably close correspondence between the experimental and theoretical results. The observed 609nm peak corresponds to the calculated 629nm excitation of the triplet, and 647nm and 623nm excitation of the quintet. The 647nm peak is smaller than the 623nm peak. The observed peak of 566nm corresponds to the 541nm excitation of the triplet and the 551nm excitation of the quintet. The largest peak seen at 409nm corresponds to the 392nm and 386nm excitations of the triplet and the 395nm and 394nm excitations of the quintet. We believe that the superposition of the triplet and quintet broadens the peaks. It should be pointed out also that the absorbance intensity of the observed peaks corresponds qualitatively to the oscillator strengths of the theoretical excitations of those experimental peaks.

In comparing our calculated results for FeTPP with the experimental results from Kobayashi and Yanagawa [34], we again see some agreement in the peak structure. Table 3.14 shows that the experimental energy difference between the double

Final Symm State	Excitation Energy (eV) Calculated	Excitation Wavelength (nm) Calculated	Oscillator Strength Calculated
$1B_2$	0.4607	2691.04	0
$1B_1$	0.4607	2691.04	0
$2B_2$	1.6492	751.79	$< 10^{-4}$
$2B_1$	1.6492	751.78	$< 10^{-4}$
$3B_1$	1.9704	629.24	0.0030
$3B_2$	1.9704	629.24	0.0030
$4B_2$	2.2909	541.21	0.0145
$4B_1$	2.2909	541.21	0.0145
$5B_1$	2.5272	490.61	0.0002
$5B_2$	2.5272	490.61	0.0002
$6B_1$	3.0033	412.83	0.0002
$6B_2$	3.0033	412.83	0.0002
$7B_2$	3.1584	392.54	0.8753
$7B_1$	3.1584	392.56	0.8753
$8B_2$	3.2112	386.10	0.1781
$8B_1$	3.2112	386.10	0.1779
$9B_1$	3.5810	346.22	0.0004
$9B_2$	3.5810	346.22	0.0004

TABLE 3.12. TDDFT calculated excitation results for the FeTPP S=1 ($^3A_2$) state.

Final Symm State	Excitation Energy (eV) Calculated	Excitation Wavelength (nm) Calculated	Oscillator Strength Calculated
$1A_2$	0.4210	2945.12	0
$1B_2$	1.5468	801.57	$< 10^{-4}$
$1B_1$	1.5472	801.36	$< 10^{-4}$
$2B_2$	1.9138	647.84	0.0014
$2B_1$	1.9140	647.78	0.0014
$3B_1$	1.9899	623.06	0.0065
$3B_2$	1.9900	623.04	0.0065
$4B_2$	2.2134	560.16	0.0001
$4B_1$	2.2139	560.04	0.0001
$5B_1$	2.2493	551.21	0.0191
$5B_2$	2.2494	551.20	0.0192
$6B_1$	3.1335	395.67	0.3249
$6B_2$	3.1336	395.66	0.3259
$7B_1$	3.1431	394.46	0.7575
$7B_2$	3.1432	394.45	0.7565
$8B_2$	3.5895	345.41	0.0260
$8B_1$	3.5897	345.39	0.0260
$9B_1$	3.6246	342.06	0.0011
$9B_2$	3.6246	342.06	0.0011
$10B_2$	3.6615	338.62	0.0221
$10B_1$	3.6618	338.59	0.0222

TABLE 3.13. TDDFT calculated excitation results for the FeTPP S=2 ($^5A_1$) state.

λ(Exp,nm)[a]	E(Exp,eV)	ΔE(Exp,eV)	λ(Calc,nm)	E(Calc,eV)	ΔE(Calc,eV)
816.33	1.5190	0.0852	801.5, S=2	1.547	0.102
772.95	1.6042		751.8, S=1	1.649	
698.69	1.7747	0.0620	629.24, S=1	1.9704	0.0196
675.11	1.8367		623.06, S=2	1.9900	
544.22	2.2785	0	551.21, S=2	2.2494	0.0415
-	-		541.21, S=1	2.2909	
444.44	2.7900	0.1627	394.46, S=2	3.1432	0.0152
419.95	2.9527		392.56, S=1	3.1584	

TABLE 3.14. Comparison of the calculated TDDFT excited states of FeTPP and the experimental absorption peaks of FeTPP in benzene.
[a] Values taken from Kobayashi and Yanagawa.[34]

peak structure agrees qualitatively with the theoretical energy difference. The first set of experimental peaks (i.e. at 816nm and 772nm) are accounted for theoretically. However, like the FeP system, the corresponding peaks are associated with small oscillator strengths, but still show a similar energy difference. As noted in the previous section the observed peak of 544nm does not show a double peak structure. However, our results suggest a double peak with at 541nm and 551nm for S=1 and S=2 respectively. This is experimentally resolved in the spectrum observed by Kobayashi and Yanagawa with FeTPP in pyridine solution which shows a double peak structure with peaks at 565nm and 532nm giving a difference on the order of 0.14eV. For each double peak seen experimentally (with the exception of the 816nm and 772nm peaks), a large theoretical oscillator strength suggests a strong excitation.

As can be seen, the TDDFT results for the FeP and FeTPP structures and our overall geometries are in good agreement with those previously published experimental and theoretical studies.

3.3.3 Charge and Spin Densities of Unsolvated FeP and FeTPP

For the triplet case of FeP and FeTPP we calculated the Mulliken spin density. The calculations suggest nearly all the α-spin density is located on the central iron atom. Around the core macrocycle there is a little α-spin density situated along the carbon atoms bonded to the nitrogen atoms which show small β-spin densities. The values for the densities are shown in Table 3.15, as well as the charge densities. From the charge densities we can see the central FeN_4 cluster of both iron complexes are negative with the surrounding eight carbon atoms being positively charged.

	S=1 FeTPP	S=1 FeTPP	S=1 FeP	S=1 FeP
Atom	Charge Density	Spin Density	Charge Density	Spin Density
Fe	0.91	2.00	0.93	2.00
N2	-0.79	-0.05	-0.77	-0.05
N3	-0.79	-0.05	-0.77	-0.05
N4	-0.79	-0.05	-0.77	-0.05
N5	-0.79	-0.05	-0.77	-0.05
C6	0.33	0.02	0.35	0.02
C7	0.33	0.02	0.35	0.02
C8	0.33	0.02	0.35	0.02
C9	0.33	0.02	0.35	0.02
C14	0.33	0.02	0.35	0.02
C15	0.33	0.02	0.35	0.02
C16	0.33	0.02	0.35	0.02
C17	0.33	0.02	0.35	0.02

TABLE 3.15. Mulliken charge densities in units of electrons per atom and spin densities for the triplet FeTPP and FeP.

3.3.4 Comparison of Unsolvated FeP and FeTPP

In the above subsections we showed the correspondence between the experimental absorption spectra of FeTPP and FeTPPS and the theoretical excitation spectra for the two iron complexes (FeP and FeTPP). We are now in a position to compare our results for the FeP and FeTPP complexes. Since the ground state is a triplet in both systems we need only compare our results for the triplet of FeP and the triplet of FeTPP.

We observe in Tables 3.6 and 3.12 the predicted absorption spectra for both systems. For nearly each peak in the FeP triplet system there is a corresponding peak in the FeTPP system. The exceptions in this case are the 715nm peak in the FeP system. We cannot be certain about the 346nm peak in the FeTPP system since we did not calculate excitations less than 350nm in the FeP calculations. In general, we find a blue shift in the spectrum of the FeP molecule relative to the FeTPP molecule. This is also seen for the quintet FeP and FeTPP as well. Both FeP and FeTPP share the same electronic configuration suggesting even further similarity between the two systems. We have already shown both the FeP and FeTPP results compare well with experimental data for FeTPP and FeTPPS.

From the charge and spin densities in Table 3.15 we see a very similar structure of the two characteristics for the FeP and FeTPP molecules. As can be seen there is very little difference numerically between the two triplet systems. Therefore, from our results, we conclude on the basis of similar electronic configurations, geometric parameters, excitation spectra, spin and charge densities that FeP can act as a substitute for the FeTPPS system. However, since our actual system is in an aqueous solution, it is necessary to study the solvent effects involving the interaction of the iron complex and the solution.

3.4 Solvated FeP Complexes

3.4.1 FeP Excited States

The interaction of FeP with the solvent in the overall process we are studying plays an important role in the electron transfer process. Smith *et. al.*[37] shows that there is an interaction between the iron complex with two water molecules– each bonded to the iron atom along the axis perpendicular to the plane. Using the B3LYP functional in their calculations, they conclude that the interaction changes the electronic configuration of the the ground state to the quintet configuration with the singlet configuration following close behind. They also conclude in terms of the functional used, that the B3LYP most accurately describes and predicts the ground state of there FeP-$(H20)_2$ complex.

The effects of this solvent on the electronic structure of FeP was treated in these calculations by way of the PCM method mentioned in Chapter 2. It has been shown by Cossi and Barone[22] that the PCM method gives better results with the explicit inclusion of two water molecules (or molecules of the solvent type) bonded to the solute molecule. In our calculations we did not explicitly include any water molecules. Another member in our group has implemented this route and his calculations be used as a comparison to what is done herein.

In the previous section, we showed that FeP can theoretically be substituted for FeTPPS in future calculations due to similarities of various properties of it and FeTPP. In Tables 3.16 and 3.17 we show the TDDFT results for the solvated triplet and quintet FeP complexes. From this data we can see the two excited state spectra, the triplet and quintet, are shifted slightly towards the blue end of the spectrum. Therefore, we would expect very similar behavior in the large iron complex of FeTPP and thus even the same in the larger FeTPPS. The $4(B_{2u}, B1u)$ states the oscillator strength has been diminished from 0.0002 in the unsolvated system to $< 10^{-4}$ in the solvated system. Therefore, we don't necessarily see the double peak structure

Final Symm State	Excitation Energy (eV) Calculated	Excitation Wavelength (nm) Calculated	Oscillator Strength Calculated
$1B_{2g}$	0.37	3332	0
$1B_{1g}$	0.37	3330	0
$1B_{1u}$	1.75	707	0.0004
$1B_{2u}$	1.75	707	0.0004
$2B_{2u}$	2.03	610	0.0046
$2B_{1u}$	2.03	610	0.0046
$3B_{1u}$	2.41	515	0.0016
$3B_{2u}$	2.41	515	0.0016
$4B_{1u}$	3.22	386	0.0470
$4B_{2u}$	3.22	386	0.0480
$5B_{1u}$	3.27	379	0.8712
$5B_{2u}$	3.27	379	0.8703

TABLE 3.16. Calculated TDDFT excitation results for the solvated FeP S=1 ($^3B_{3g}$) state.

Final Symm State	Excitation Energy (eV) Calculated	Excitation Wavelength (nm) Calculated	Oscillator Strength Calculated
$1B_{3g}$	0.23	5389	0
$1B_{1g}$	0.45	2732	0
$1B_{2g}$	0.45	2732	0
$1B_{2u}$	1.70	730	$< 10^{-4}$
$1B_{1u}$	1.70	730	$< 10^{-4}$
$2B_{1u}$	2.03	610	0.0024
$2B_{2u}$	2.03	610	0.0024
$3B_{2u}$	2.38	521	0.0001
$3B_{1u}$	2.38	521	0.0001
$4B_{2u}$	3.21	386	$< 10^{-4}$
$4B_{1u}$	3.21	386	$< 10^{-4}$
$5B_{2u}$	3.27	379	0.9865
$5B_{1u}$	3.27	379	0.9867
$6B_{2u}$	3.69	336	0.0268
$6B_{1u}$	3.69	336	0.0269
$7B_{2u}$	3.78	328	0.0181
$7B_{1u}$	3.78	328	0.0179

TABLE 3.17. Calculated TDDFT excitation results for the solvated FeP S=2 (^5A_g) state.

at or around the 386nm peak as the $4(B_{2u}, B1u)$ appears very weak. On the same note, we do see for the $5(B_{2u}, B1u)$ an increased oscillator strength compared to the unsolvated system, which is seen experimentally to be a strong peak.

3.4.2 Solvated FeP Spin and Charge Densities

In looking at the charge and spin densities of the triplet and quintet in Table 3.18, we see very similar values for each atom making up the macrocycle, except for the iron atom. The N_4 cluster is negative, while the remaining macrocycle is positive. For the iron, we see most of the spin is located on the iron atom itself. Compared to the values of the unsolvated system we see a very similar trend in values of the charge and spin density.

Atom	S=1 FeP Charge Density	S=1 FeP Spin Density	S=2 FeP Charge Density	S=2 FeP Spin Density
Fe	0.93	2.00	1.10	3.73
N2	-0.77	-0.05	-0.80	0.03
N3	-0.77	-0.05	-0.80	0.03
N4	-0.77	-0.05	-0.80	0.03
N5	-0.77	-0.05	-0.80	0.03
C6	0.32	0.02	0.33	0.02
C7	0.32	0.02	0.33	0.02
C8	0.32	0.02	0.33	0.02
C9	0.32	0.02	0.33	0.02
C14	0.32	0.02	0.33	0.02
C15	0.32	0.02	0.33	0.02
C16	0.32	0.02	0.33	0.02
C17	0.32	0.02	0.33	0.02

TABLE 3.18. Mulliken charge densities in units of electrons per atom and spin densities for the triplet and quintet FeP.

CHAPTER 4

Excited State Electron Transfer

4.1 Introduction

In this chapter, we give the general idea behind excited state electron transfer and discuss the topics associated with this process. The thermodynamics that govern this process will be given. The PCM method will be applied to our system involving the aqueous FeP-TNT interaction.

In Chapter 3 the theoretical excited state structure was given. Knowing the excited states of a molecule or an atom, in part, can help determine if electron transfer can occur. As will be shown below, the excitation energy is used to calculate the change in Gibbs free energy of the system. Of course the excited state alone will not tell you this – more knowledge is necessary. However, the excited state is a good place to start in understanding an ET process. For now, the reader should know that for an arbitrary chemical species, a letter will be used to designate the ground state, for instance A. If the chemical complex is in its excited state, the designation A* will be given.

In the ground state of a complex, the energy of each molecule is in its respective minima. In other words, the geometry and electronic arrangement are in such a configuration as to give the lowest energy of the system. The lowest possible vibration level, denoted as the zero-point level, is normally more populated at room temperature than the higher excited vibrational levels because the thermal energy of k_bT is only $0.0257eV$.[38] This energy is enough to agitate the system into this lowest vibrational state.

As with every complex there are vertical excited states (electronic excitations) to which the system is promoted with the absorption of a photon. This promotes the system from some vibrational state of the electronic ground state to another vibrational state in a higher energetic electronic state. During the the absorbance of a photon by an electron, the nuclear geometry of the complex does not normally change.[38] The electron is much less massive then the nucleus and therefore the excitation process can be approximated in this way (that the geometry doesn't change initially with an excitation occurring). This is the well known Frank-Condon principle. The time in which the vertical transition occurs is on the order of $10^{-16}s$. The time for the nuclear vibrational transition is on the order $10^{-14} - 10^{-12}s$.[38] In other words, what is taking place is an absorption of a photon by an electron. This promotes the electron to an excited state or what is known as a Frank-Condon state. After the excitation occurs, the nuclear geometry relaxes due to the change in electron density until an equilibrium is found. This relaxation lowers the energy slightly, compared to the Frank-Condon state, and can be long-lived. This is illustrated in Fig. 4.1.[39] It is the relaxed excited state that is responsible for participating in a photochemical reaction.

Once a complex is in its excited state configuration, it can decay back into its lower energy state in 3 different ways. The process can be nonradiative in which case there is a release of heat due to lattice vibrations. Radiative processes involve the emission of a photon through decay into lower states. Then there is fluorescence which is the decay from the lowest vibrational state of the excited state into another vibrational state of a lower electronic state, accompanied by light emission. Since some of the energy of the excited state goes into the vibration of the lattice, there will be a decrease in the energy emitted from the decay of the electronic excited state to a lower state. Thus the wavelength for the emission process will be longer corresponding to that for the absorption process. The difference in these wavelengths is known as the Stokes shift.

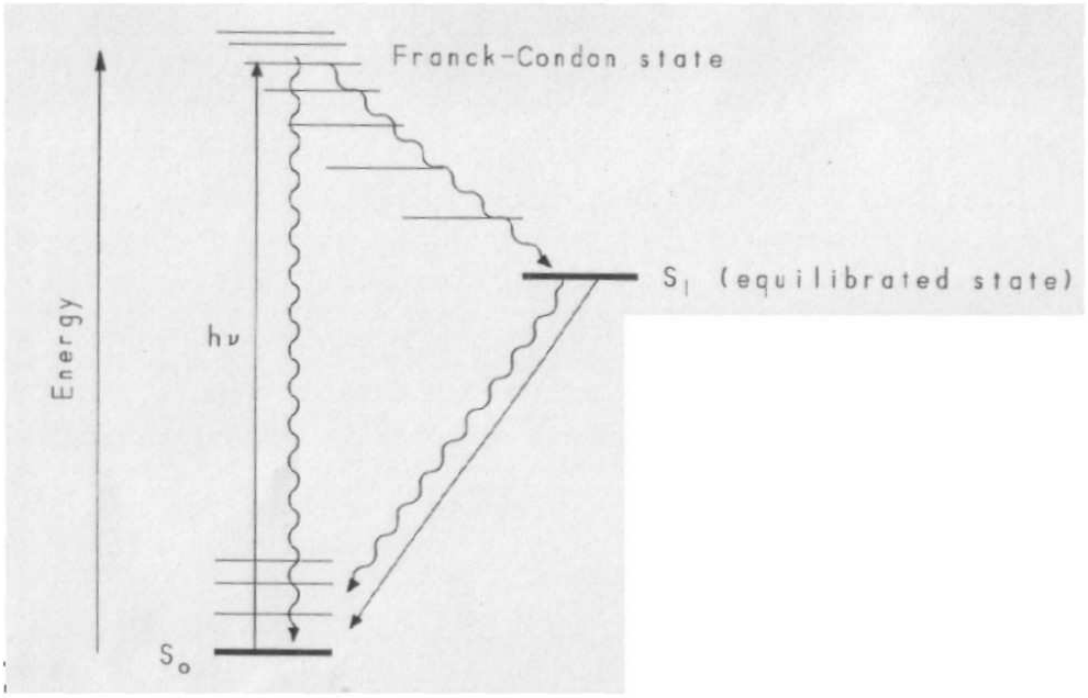

Figure 4.1. Excitation of the electron to the Frank-Condon state which then relaxes to the equilibrated state.

4.2 Thermodynamic Factors of Photoinduced Electron Transfer

4.2.1 Quenchers and Sensitizers

Thermodynamics describes the reaction between two molecules and can be used to determine if the reaction will proceed forward. To better understand these reactions a knowledge of the thermodynamics governing the reactions themselves must be taken into account. The emphasis in this section will primarily be the energetics of reactions. The notation used will follow that of Kavarnos.[38]

If a molecule is excited electronically and the excited state is long lived, it is possible for another molecule in its ground state to interact with the excited molecule and cause an electron transfer. The excited molecule will be known as the sensitizer and the interacting ground state molecule will be known as the quencher. The sensitizer can cause changes in the quencher through an electron transfer. The effect of the quencher is to quench, or deactivate the excited molecule the sensitizer.

As mentioned above we have two complexes that are interacting with each other which can be written as the following

$$D^* + A \xrightarrow{E_\lambda} D + A^* \tag{4.1}$$

where D^* represents the electron donor which is the excited state sensitizer. A is the electron acceptor which is the quencher, and A^* is the excited state acceptor. Another way to see the reaction is to include the photoexcitation of the donor D. Thus we have

$$D^m + A^n \xrightarrow{k_{h\nu}} [D^m]^* + A^n \xrightarrow{k_{\text{en}}} D^{m+1} + A^{n-1} \tag{4.2}$$

The first reaction is the photoexcitation of the donor. Then the proceeding step is the donor giving an electron from its excited state to the acceptor. This is seen as the overall charge on the donor is increased by $+1$ and the acceptor is decreased by -1, where m and n represent the initial charge of the molecule.

4.2.2 Enthalpy and Gibbs Free Energy

It is important to know the Gibbs free energy change which will tell us whether or not the system will need energy to proceed or is a spontaneous process. The free energy change accompanying a chemical process is given by

$$\Delta G = \Delta H - T\Delta S \tag{4.3}$$

where ΔG is the Gibbs free energy change and ΔH is the heat of enthalpy. T and ΔS are the absolute temperature and change in entropy, respectively.

In the process of the donor system going from its ground state D to its excited state D^* and then to its donor state D^+, we can write the heat of enthalpy as $\Delta H_{D^* \rightarrow D^+}$ – an exothermic reaction. The process of the system going from its ground state D to is donor state D^+ gives the heat of enthalpy as $\Delta H_{D \rightarrow D^+}$ – an endothermic reaction.

This can be seen from Fig. 4.2 [40] and the energy E_{00}^D can be written in terms of the heats of enthalpy as

$$-\Delta H_{D^* \longrightarrow D^+} + \Delta H_{D \longrightarrow D^+} = E_{00}^D. \tag{4.4}$$

Using this equation in conjunction with the Gibbs free energy equation we can rewrite E_{00}^D as

$$E_{00}^D = -\Delta G_{D^* \longrightarrow D^+} - T\Delta S_{D^* \longrightarrow D^+} + \Delta G_{D \longrightarrow D^+} + T\Delta S_{D \longrightarrow D^+}. \tag{4.5}$$

If we neglect the $T\Delta S$ terms since their contribution will be small due to small structural changes in going from $D \longrightarrow D^* \longrightarrow D^+$ thus making ΔS negligible, the free energy change is given by

$$\Delta G_{D^* \longrightarrow D^+} = \Delta G_{D \longrightarrow D^+} - E_{00}^D. \tag{4.6}$$

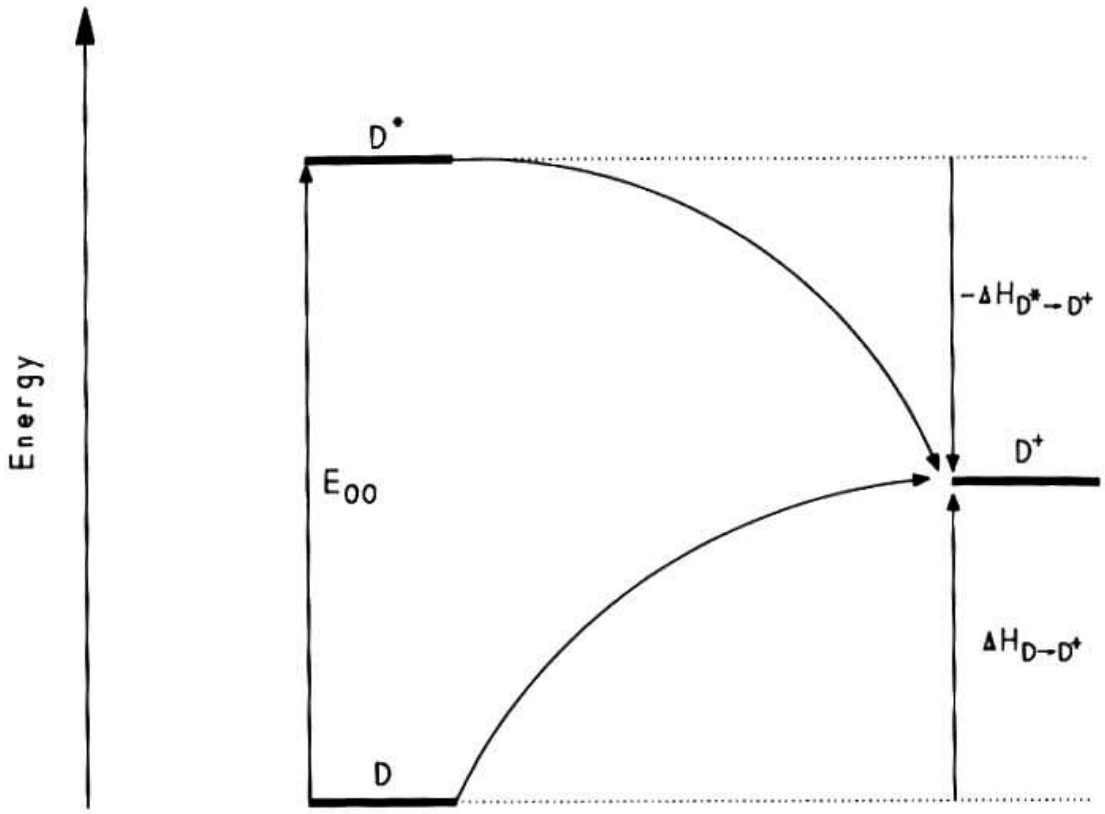

Figure 4.2. Enthalpy changes of the donor complex.

In keeping with the above prescription, we can find the free energy associated with the reduced acceptor system A. We can write this as

$$\Delta G_{A^* \longrightarrow A^-} = \Delta G_{A \longrightarrow A^-} - E^A_{00}. \tag{4.7}$$

If we look at the half reactions of the donor and acceptor complexes, for which the free-energy change was found, we can introduce the free-energy in terms of the redox potential (also known as the electromotive force or emf) or E_{redox}. As is customary the half-reactions will be written as reductions so that we have the following

$$D^+ + e^- \longrightarrow D \tag{4.8}$$

$$A + e^- \longrightarrow A^-. \tag{4.9}$$

Now in reference to the half-reactions we can write

$$\Delta G = -nFE_{redox}. \tag{4.10}$$

where n is the number of moles of e^- transferred and F is number of electrons per mole (known as the Faraday).

4.2.3 Redox Potentials

Now that we have the Gibbs free energy written in a compact form we can write the redox potentials for the half-reactions involving the excited state. This gives

$$E_{D^* \longrightarrow D^+} = E_{D \longrightarrow D^+} + E^D_{00} \tag{4.11}$$

$$E_{A^* \longrightarrow A^-} = E_{A \longrightarrow A^-} - E^A_{00}. \tag{4.12}$$

We can rewrite these redox potentials in a simpler form by using the notation $E^0(D^+/D) = -E_{D\rightarrow D^+}$ and $E^0(D^+/D^*) = -E_{D^*\rightarrow D^+}$ and similar for the other potentials. Now we can rewrite the potentials as

$$E^0(D^+/D^*) = E^0(D^+/D) - E^D_{00} \tag{4.13}$$

$$E^0(A^*/A^-) = E^0(A/A^-) + E^A_{00}. \tag{4.14}$$

As was mentioned previously, the excited state is better suited for electron transfer than its ground state. This is seen above where $E^0(D^+/D^*) < E^0(D^+/D)$. In short, the lower the $E^0(D^+/D^*)$ of the complex the easier the donor can donate an electron from its excited state.

Up to this point we have taken the individual energies of the donor and acceptor complexes to develop the energetics. Now we are in a position to combine the two complexes and find the energy necessary to determine the viability of electron transfer within a solution. Figure 4.3[41] can be our guide to determine the free energy changes associated with the electron transfer process from the excited state donor complex. The free energy changes for the uphill reaction can be written as

$$\Delta G^{up}_{el} = \Delta G_{D\rightarrow D^+} + \Delta G_{A\rightarrow A^-}. \tag{4.15}$$

For the downhill reaction, which is where the ET takes place, we can write the free energy change of the donor-acceptor complex as

$$\Delta G^{down}_{el} = \Delta G_{D^*\rightarrow D^+} + \Delta G_{A\rightarrow A^-}. \tag{4.16}$$

If we rewrite our equation in terms of the reduced half reactions we obtain

$$\Delta G^{down}_{el} = nF[E^0(D^+/D^*) - E^0(A/A^-)]. \tag{4.17}$$

Now with the substitution of $Eq.31$ the above expression yields

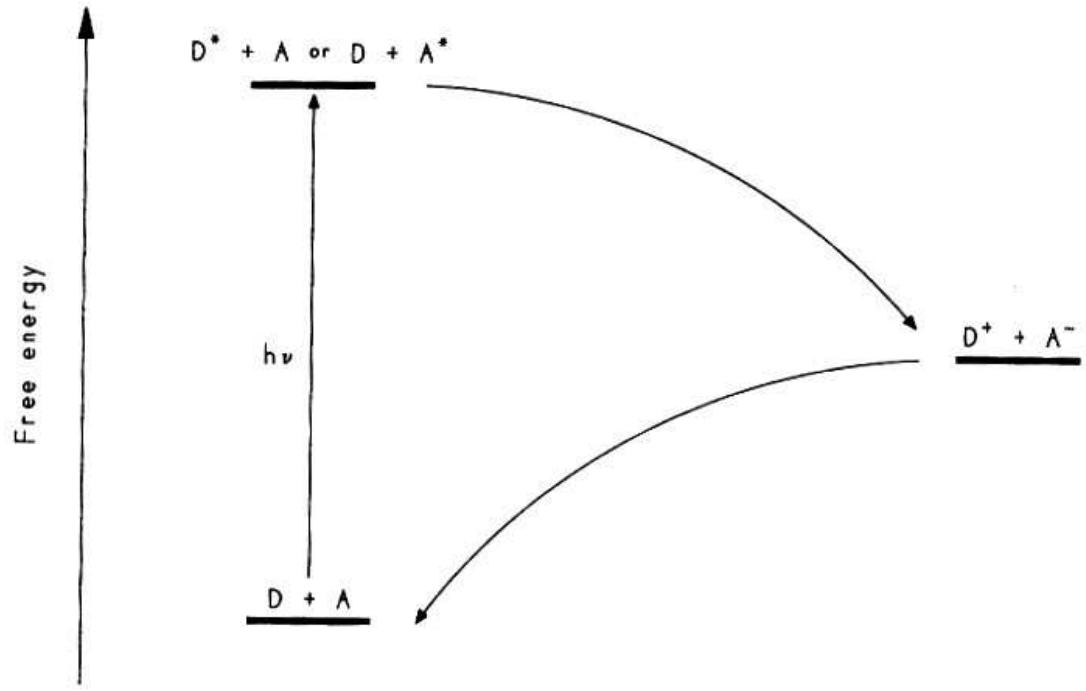

Figure 4.3. Energy diagram for photoinduced electron transfer.

$$\Delta G_{el}^{down} = nF[E^0(D^+/D) - E^0(A/A^-)] - \Delta E_{00}^D. \tag{4.18}$$

Changing units to $kcal \cdot mol^{-1}$, using the fact that for most one-electron transfers we have $nF \sim 1$, and using direct substitution of the expression for $E^0(D^+/D^*)$ leads to

$$\Delta G_{el}^{down} = 23.06[E^0(D^+/D) - E^0(A/A^-)] - \Delta E_{00}^D. \tag{4.19}$$

where ΔE_{00}^D is the excitation energy corresponding to the equilibrated energy E_{00}^D and is measured in eVs. The coefficient 23.06 $kcal \cdot mol^{-1}$ comes from $(3.82929 \cdot 10^{-23} kcal)N_A$ where N_A is Avagadro's number.

Assuming now that instead of two initially charged complexes we have two neutral complexes in which electron transfer will take place. After electron transfer there will be two charge complexes D^+ and A^-. Due to the formation of this ion pair, coulombic attraction between these final charged complexes will pull them together thus releasing energy denoted by w_p. Therefore, we should modify the Eq. 4.19 to include this work term w_p. We can write w_p as

$$w_p(kcal \cdot mol^{-1}) = \frac{332(z_{D^+} z_{A^-})}{d_{cc}\epsilon_s} \tag{4.20}$$

where we define z_{D^+} and z_{A^-} as the molecular charges, ϵ_s as the static dielectric of the solvent, and d_{cc} as the center-to-center separation distance between donor-acceptor complexes in $\mathring{A}$.[38] The coefficient 332 comes from computing $N_A e^2/4\pi\varepsilon_0$ and changing to $kcal$. With the inclusion of this modification we can arrive at what is known as the Rehm-Weller equation[42] given as

$$\Delta G_{el}^{down} = 23.06[E^0(D^+/D) - E^0(A/A^-)] - w_p - \Delta E_{00}^D. \tag{4.21}$$

In short, the Rehm-Weller equation states that $\Delta G_{el} < 0$ for spontaneous electron transfer between uncharged reactants. This equation can be used as a tool to determine the energetic feasibility of ET taking place with the given system.[43]

In our *ab initio* study of the FeP-TNT system, we did not include the empirical values for the oxidation and reducion potentials that are be used in Eq. 4.21. Instead, however, we calculated the free energies of the molecules we believe are involved in the electron transfer process. Therefore, Eq. 4.16 is modified to give us a working equation that enables us to find the Gibbs free energy of the system by using the individual molecular free energies. Substituting Eq. 4.6 into Eq. 4.16 and including the the coulombic term w_p gives us this more usable equation in terms of calculated values of the free energies written as

$$\Delta G_{el}^{down} = \Delta G_{D\rightarrow D^+} + \Delta G_{A\rightarrow A^-} - \Delta E_{00}^{D} - w_p. \tag{4.22}$$

From Eq. 4.22 it can now be seen that we need only find the molecular free energies in the solvated system, the excited state involved in the electron transfer, and the coulombic interaction of the solvated donor-acceptor complexes. This data is presented in the next chapter.

CHAPTER 5

Excited State Electron Transfer Results

5.1 Introduction

In Chapter 4 the thermodynamic expressions needed to determine the Gibbs free energy were developed. From this we can predict whether or not the thermodynamic condition exists for electron transfer to proceed in the system we are studying, i.e. $\Delta G_{el}^{down} < 0$, by using Eq. 4.22. In this chapter, the probable reaction pathway will be given, as well as the calculated free energies for each complex. From there, Eq. 4.22 will be used to show the possibility of electron transfer for this particular pathway of our FeP-TNT system.

In this system, FeP acts as the sensitizer, and TNT acts as the quencher. Since our previous calculations agree with previously published data on the matter of the ground state of FeP being a triplet, we will use this triplet state as the basis for the calculations done herein. Since both the reaction involving FeP and TNT occurs in an aqueous solution we need to take into consideration the solvent effects.

This interaction is taken care of by using a method developed by Cossi and Barone.[22] The method used is called the PCM method which utilizes overlapping spheres to generate a spherical cavity to account for the water solution in which the system will be submerged, as was discussed in Chapters 2 and 3. It is, however, possible that instead of electron transfer from FeP to TNT we can have just the opposite take place–electron transfer from TNT to the FeP. Since visible light is the driving force behind this process and FeP is excited with visible light as seen in Fig. 3.1, FeP was initially thought of as being the excited molecule in which the

electron transfer process was initiated. Therefore, we did not investigate electron transfer from TNT to FeP. In this thesis, only electron transfer from FeP to TNT will be discussed and the proposed pathway is given by

$$\begin{aligned} FeP(S=1)+TNT(S=0)) &\xrightarrow{E_\lambda} [FeP(S=1)]^* + TNT(S=0) \\ &\longrightarrow [FeP]^{+1}(S=3/2) + [TNT]^{-1}(S=1/2) \\ &\xrightarrow{O_2} R-COOH(S=0) + FeP(S=1) + H_2(S=0) \\ &\longrightarrow TNB(S=0) + CO_2(S=0) \end{aligned} \tag{5.1}$$

where R represents the ligated trinitrobenzene, and TNB is just trinitrobenzene.

5.2 Calculations

The ionized iron complex has three different spin states possible for the ground state. Our calculations show the S=3/2 state is the ground state with the S=1/2 being slightly above, and the S=5/2 being even higher in energy. These results are consistent with previous work from Smith et. al..[37] We believe this S=3/2 spin state for FeP^{+1} is associated with the electron transfer pathway due to it being the ionized ground state. In looking at the mapping of the electronic charge densities for both the solvated FeP triplet in Fig. 5.1 and the FeP S=3/2 (ionic FeP) in Fig. 5.2 we can see that the Fe atom is less negative in the ionized FeP. This is an indication that the most of the charge associated with the electron transfer is coming from the iron with a small contribution from the macrocycle. The electronic configuration can point us in the direction as to which occupied orbital the transferred electron is coming from. Table 5.1 shows the configurations FeP and FeP^{+1}. From this, we can see that the electron is predominately coming from the d_{z^2} orbital.

Figures 5.3 and 5.4 show the effective charges at each atomic site using the Mulikin population analysis. Comparing these charge density maps of the TNT and TNT^{-1} shows how the charge distribution changes from the initial ground state to the

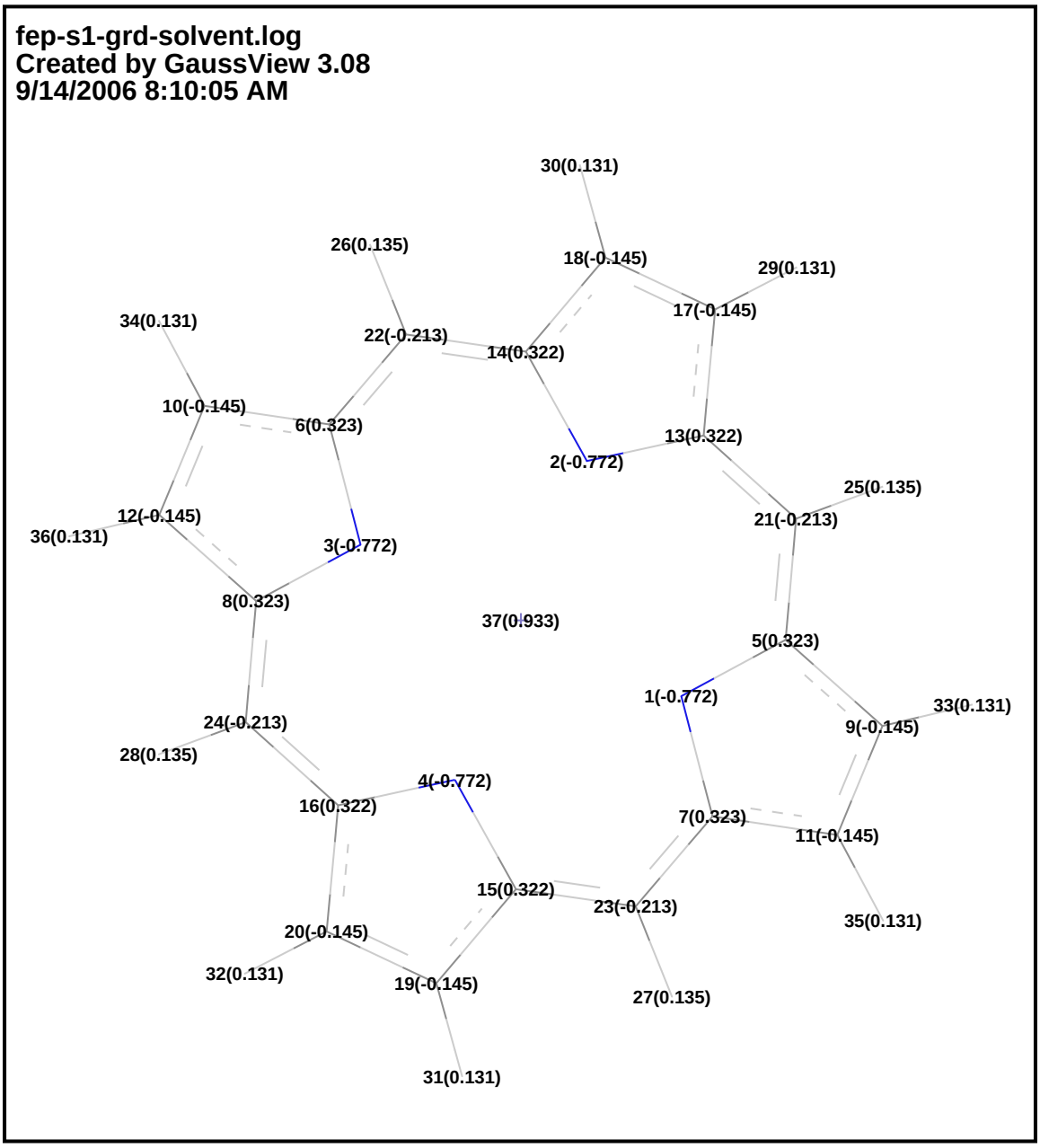

Figure 5.1. Model of solvated FeP triplet charge density map. This model is used as a reference diagram for the atomic charges.

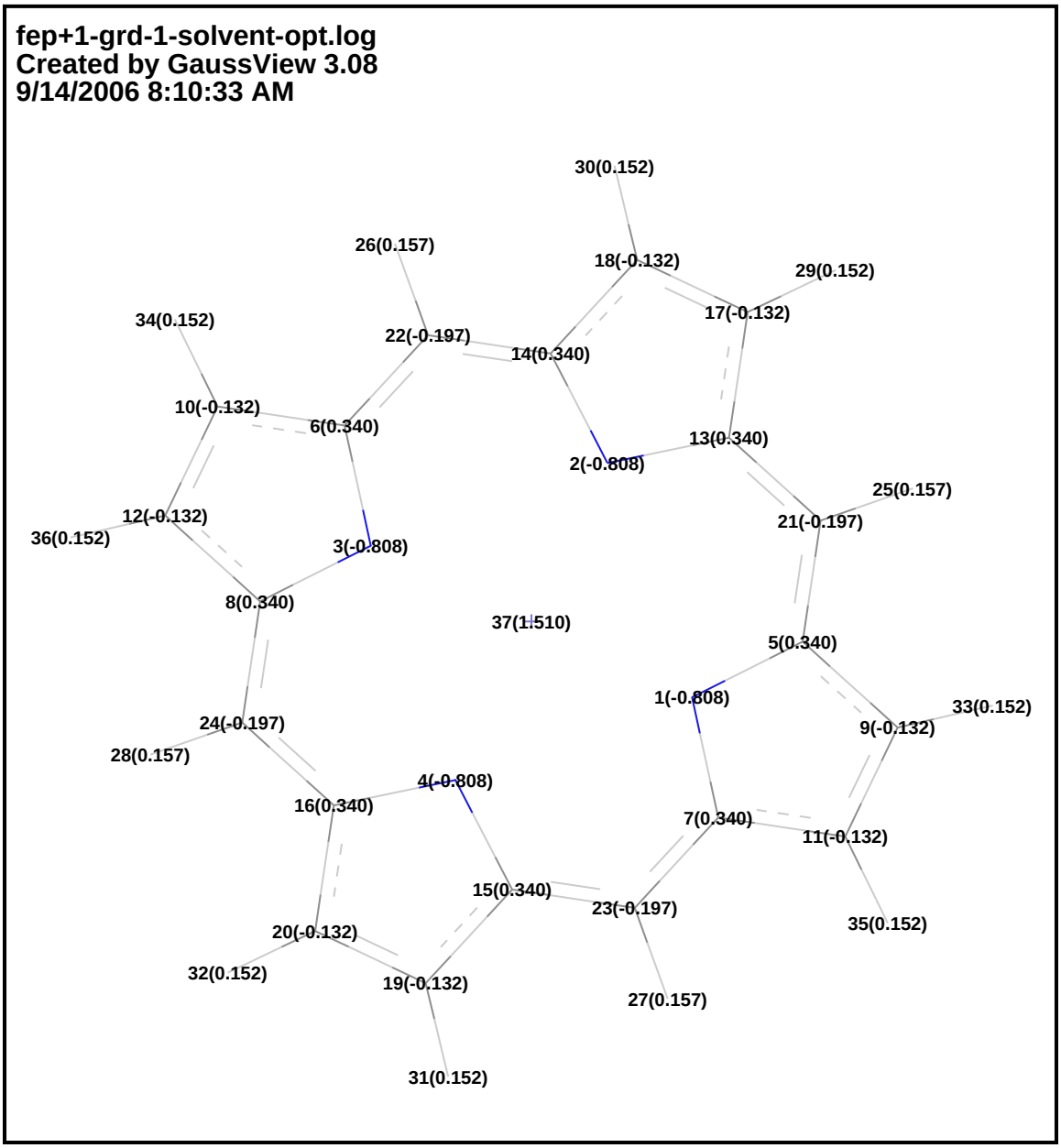

Figure 5.2. Model of solvated FeP S=3/2 charge density map. This model is used as a reference diagram for the atomic charges.

	d_{z^2}	d_{xy}	d_{xz}	d_{yz}	$d_{x^2-y^2}$
FeP	2	2	1	1	0
FeP^{+1}	1	2	1	1	0

TABLE 5.1. Table giving the occupied orbitals of the FeP and FeP^{+1} complexes.

ionic state. As can be seen, much of the charge is transferred to the oxygen atoms of the NO_2 groups. Atom 15N is the only nitrogen atom that appears to have noticeably decreased in charge indicating a slight deposit of of the electronic charge, which is in agreement with works done by Huang and Leszczynski.[44] The map also shows the atoms in the C-H bonds in the benzene ring have change more then the other carbon atoms in the ring. The atoms in the C-CH_3 bond show the ring-carbon atom to have increased in negativity while the carbon atom in the CH_3 group has become slightly more positive then its initial counterpart. It is possible that this change in the charge of the bonding atoms will weaken the C-CH_3 bond.

We chose to focus our calculations on ET from FeP to TNT due to the experimental evidence that showed FeP has the same excitation wavelengths as the light being used to initiate the process. From the experimental results, it was found that 90% of the initial amount of TNT (in the TNT-FeTPPS) solution was deactivated in a period of less than one hour.[45] So the process has been verified to work experimentally. However, the ET pathway by which the process takes place is not yet understand and is the subject of this investigation.

5.3 Thermodynamic Calculations

For our system were were able to calculate the free energies for each molecule we believe are involved in the process of electron transfer. Table 5.2 shows the free energies associated with each component in the reaction given by Eq. 5.1.

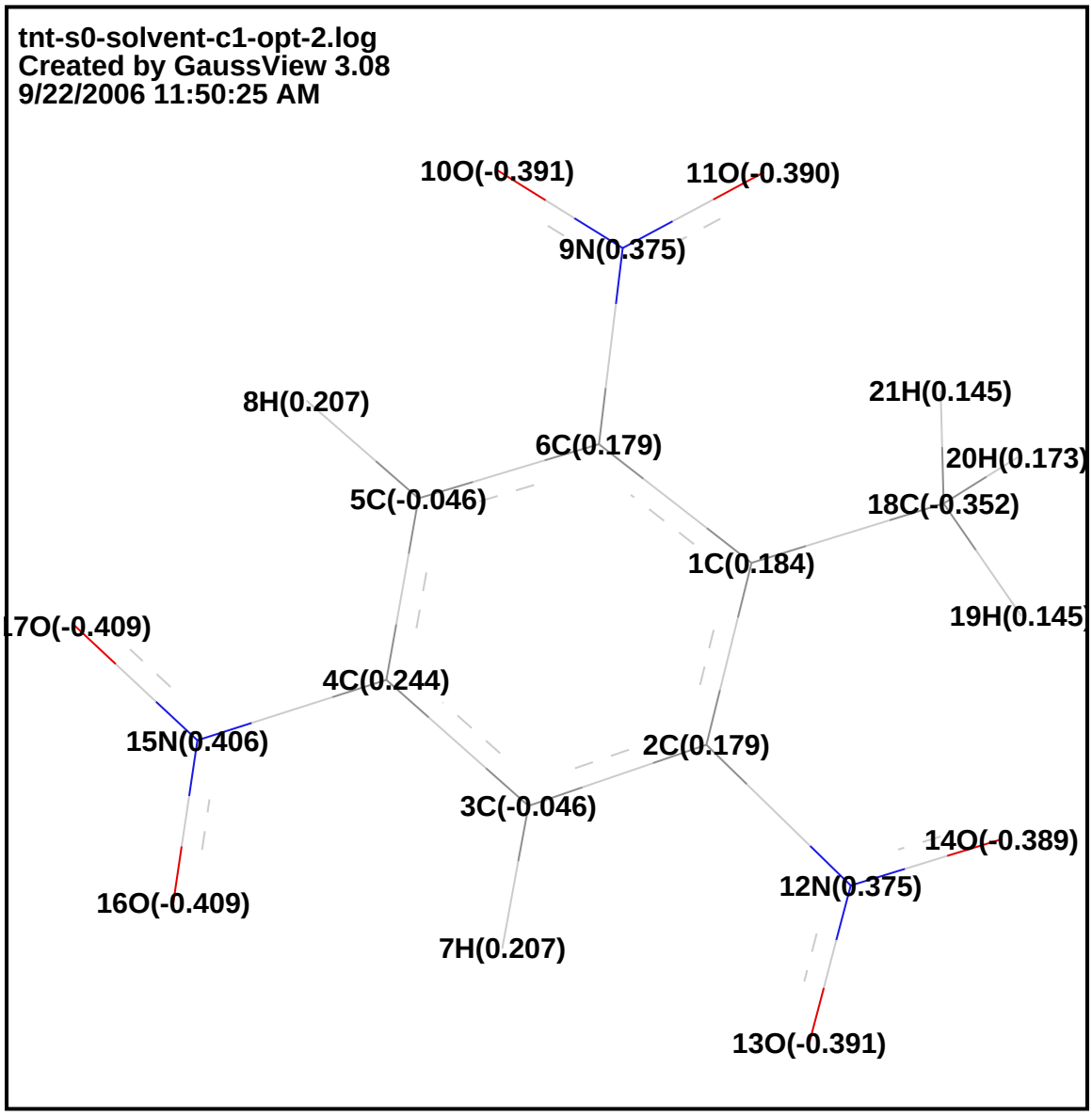

Figure 5.3. Model of solvated TNT S=0 charge density map. This model is used as a reference diagram for the atomic charges.

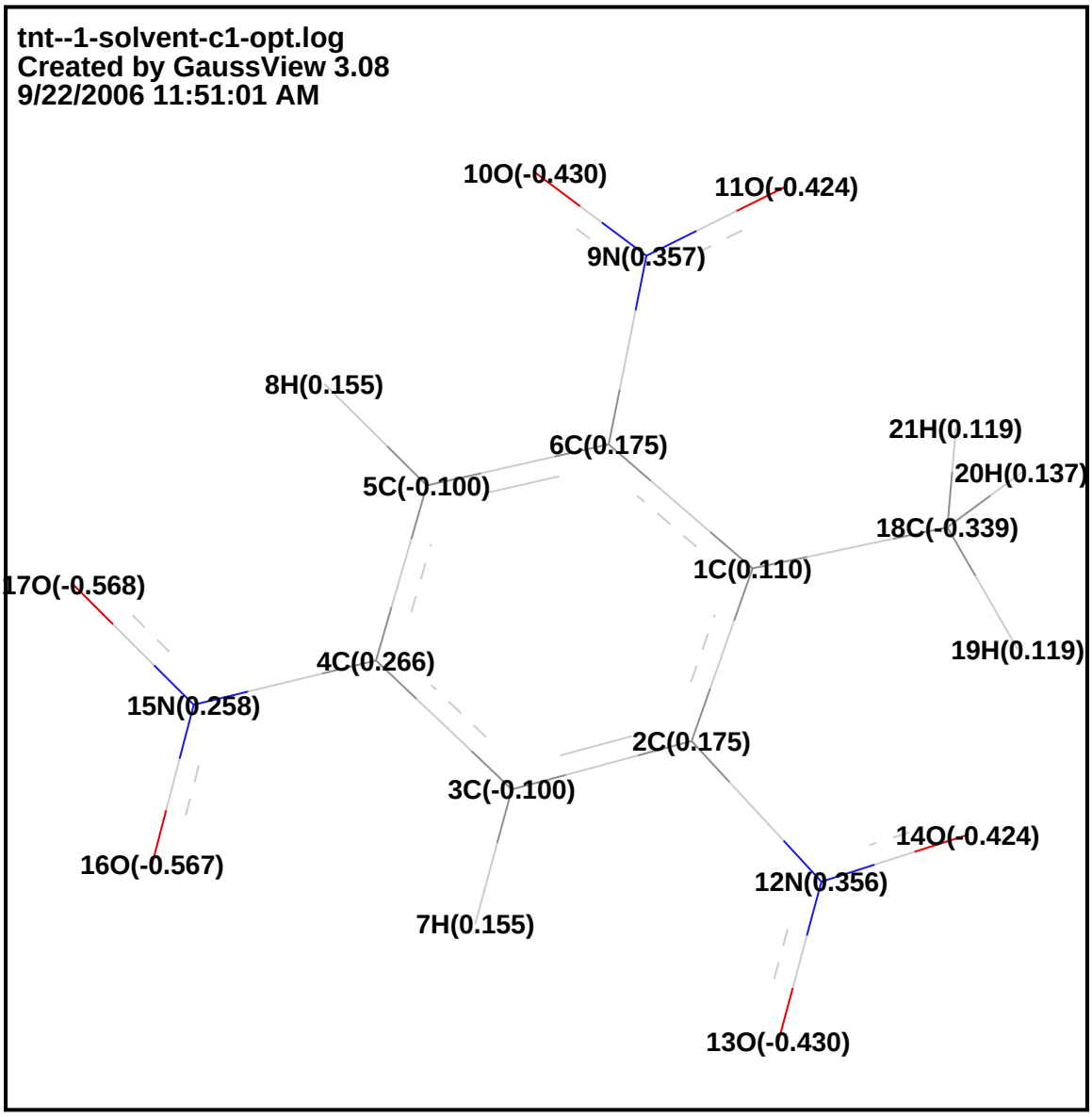

Figure 5.4. Model of solvated ionic TNT S=1/2 charge density map. This model is used as a reference diagram for the atomic charges.

For simplicity, the reaction in Eq. 5.1 will be broken up into three parts: RXN 1, RXN 2, and RXN 3. Each reaction will be defined in the following way:

$$\begin{aligned} RXN\ \ 1: \quad FeP(S=1) \quad + \quad TNT(S=0) &\xrightarrow{E_\lambda} [FeP(S=1)]^* + TNT(S=0) \\ &\longrightarrow \quad [FeP]^{+1}(S=3/2) + [TNT]^{-1}(S=1/2) \end{aligned} \tag{5.2}$$

$$\begin{aligned} RXN\ \ 2: \quad [FeP]^{+1}(S=3/2) \quad + \quad [TNT]^{-1}(S=1/2) &\xrightarrow{O_2} R-COOH(S=0) \\ +FeP(S=1) \quad + \quad H_2(S=0) & \end{aligned} \tag{5.3}$$

$$RXN\ \ 3: \quad R-COOH(S=0) \longrightarrow TNB(S=0) + CO_2(S=0). \tag{5.4}$$

In RXN 1, there are a few steps involved and the free energies are not calculated for each step. The reason for this is that the donor free energy term in ΔG_{el}^{down} only involves the ground state of FeP and its ionized state FeP^{+1}. Therefore, even though the excited state term exists in the reaction, it is accounted for in Eq. 4.22 by the explicit excitation energy E_{00}^{D}. By plugging in the values necessary for RXN 1, given in Table 5.2, we can find out if electron transfer is likely to occur by taking into account the thermodynamic condition of spontaneity for $\Delta G < 0$. Using Eq. 4.22 we see the term w_p which is the work term as mentioned previously. However, remembering the work term is inversely proportional to the distance between the ionized donor and acceptor, and is also subtracted from the total free energy, it can be seen that this term only serves to make the free energy more negative with a smaller distance. Calculations including the FeP and TNT molecules with the inclusion of a water cage have been performed by Scofield[46] whose calculations show, at this junction, that the FeP is separated from the TNT by a couple of water molecules. The distance given

between the two complexes on average is on the order of 5.7Å[46] due to a slight tilt of the TNT by 33.4° on the face to face orientation. Therefore, using a value of d_{cc}=5.7 and ε_s=80.2 we find

$$w_p = \frac{14.40}{d_{cc}\varepsilon_s} = 0.03 \;\; eV. \tag{5.5}$$

Using this value for the free energy expression, we find

$$\Delta G_{el}^{down}(eV) = \Delta G_{D\rightarrow D^+} + \Delta G_{A\rightarrow A^-} - \Delta E_{00}^{D} - w_p = -2.23 \;\; eV. \tag{5.6}$$

Therefore, we can see there is spontaneity in the the electron transfer from FeP* to TNT. The excited energy used for E_{00}^{D} is that taken from the solvated excitation spectrum of the triplet FeP in Table 3.6 and is the excited state with the largest oscillator strength, i.e. the $5(B_{1u}, B_{2u})$ state also known as the Q-band. Although the equilibrated excited state of FeP participates in the electron transfer process, the excitation energy used is not that of the relaxed excited state, but the Frank-Condon state. In our calculations it is not possible to find the equilibrated energy for this particular excited state using TDDFT because of the symmetry state held by this excitation. Lower energy excitations also have the same symmetry and thus optimizing this particular state will only optimize the first excited state with the same symmetry and not the excited state we believe is involved in the electron transfer process. However, we can estimate the value of the equilibrated excited state in a limiting way by take the difference between the lowest allowed excitation and the Q-band. This gives a value of 1.5 eV. In short, calculating the ΔG for RXN 1 shows in a somewhat simplified manner in which electron transfer is likely to occur.

As for whether or not the entire pathway proposed is an energetically favorable pathway, we must also find the Gibbs free energy for RXN 2 and RXN 3. The individual molecular free energies can be found from Table 5.2 as well. Table 5.3 shows a summary of these change in free energies. We can see from Table 5.3 that in

Molecule	Gibbs Free Energy (au)
$FeP(S=1)$	-2251.889359
$FeP^{+1}(S=3/2)$	-2251.733281
$TNT(S=0)$	-884.976404
$TNT^{-1}(S=1/2)$	-885.108219
$O_2(S=1)$	-150.336406
$H_2(S=0)$	-1.180059
$R-COOH(S=0)$	-1034.247947
$TNB(S=0)$	-845.693313
$CO_2(S=0)$	-188.589561

TABLE 5.2. Gibbs free energies for each molecule in the electron transfer process.

Reaction	ΔG(eV)
RXN 1	-2.23
RXN 2	-3.80
RXN 3	-0.95

TABLE 5.3. Change in Gibbs free energies for each set of reactions in the electron transfer process.

each set of the overall proposed reaction in Eq. 5.1, the processes is thermodynamically favorable as given by the thermodynamic condition of spontaneity.

CHAPTER 6

Summary and Conclusion

In chapter 2 the theory for the first part of my calculations was presented mainly dealing with DFT and TDDFT with a short discussion on the CIS, and PCM method used to account for the aqueous solvent used. In chapter 3 I presented our results involving different aspects of the calculations. We showed that our results involving symmetry, geometry, energetic orderings, and electronic configurations are consistent with those found by other groups. We also showed the excitations predicted by TDDFT and CIS of the different multiplets of the unsolvated FeP and FeTPP (TDDFT only) complexes. A comparison was given showing the theoretical excitations of FeP and the experimental absorption spectrum FeTPPS. The excitations of FeP showed there was a direct correlation to the experimental absorption spectrum of FeTPPS, accounting for the observed peaks in our calculations through the electronic dipole allowed transitions. From this we saw the theoretical excitation spectrum of FeP was blue shifted by approximately 30 nm. We found from comparing the larger FeTPPS complex to the smaller FeP complex that FeP was able to be to substituted in for FeTPPS, in terms of computational convenience.

Calculations performed on the larger FeTPP complex (FeTPPS minus the sulfonate groups) show that FeP has a very similar charge density and spin density for the the two molecules. In addition, the theoretical experimental spectra of the two molecules further shows the similarities of the two molecules, suggesting more so that FeTPPS can be substituted by FeP in terms doing calculations. We also presented our results including the solvent for the FeP molecule, given in Chapterr 3. From this we showed the theoretical excitation spectrum was slightly blue shift as a result

while maintaining the a qualitative agreement with the observed peaks. Therefore, it is our belief that FeP can be used in place of FeTPPS in future calculations.

In chapter 4 I presented Gibb's free energy condition of spontaneity. I showed that instead of using redox potentials, we could in fact use the free energies resulting from our calculations. Chapter 5 gives a suggested pathway in which to photodeactivate TNT by way of FeTPPS. Using the free energy idea and a form of the Rehm-Weller equation, chapter 5 gives the results of the free energies calculated within the solvated system to more accurately account for solvent-solute interactions. It it shown that the proposed pathway for the degradation of TNT is thermodynamically favorable. Taking these ideas into consideration and what has been presented in chapters 3 and 5, I believe the proposed pathway is the likely pathway for the process studied by Harmon *et. al.*.[11,32]

BIBLIOGRAPHY

1. Charles Michael Drain, Joeseph T. Hupp, Kenneth S. Suslick, Michael R. Wasielewski, Xin Chen, J. Porphyrins and Phthalocyanines 6, 243 (2002).

2. B. Delly, Physica B, 172, 185 (1991).

3. Carme Rovira, Pietro Ballone, Michele Parrinello, Chem. Phys. Lett., 271, 247 (1997).

4. Pawel M. Kozlowski, Thomas B. Spiro, Attila Bérces, Marek Z. Zgierski, J. Phys. Chem. B, 102, 2603 (1998).

5. Marie-Madeleine Rohmer, Chem. Phys. Lett., 116, 44 (1985).

6. Carme Rovira, Karel Kunc, Jrg Hutter, Pietro Ballone, Michele Parrinello, J. Phys. Chem. A, 101, 8914 (1997).

7. Yoong-Kee Choe, Tomohiro Hashimoto, Haruyuki Nakano, Kimihiko Hirao, Chem. Phys. Lett., 295, 380 (1998).

8. James P. Collman, J. L. Hoard, Nancy Kim, George Lang, Christopher A. Reed, J. Am. Chem. Soc., 97, 2676 (1975).

9. Shigeru Obara and Hiroshi Kaskiwagi, J. Chem. Phys., 77, 3155 (1982).

10. Harold Goff, Gerd N. La Mar, Christopher A. Reed, J. Am. Chem. Soc., 99, 3641 (1977).

11. H.J. Harmon, Chemosphere 63, 1094 (2006).

12. Attila Szabo and Neil S. Ostlund, in *Modern Quantum Chemistry: Introduction to Advanced Electronic Structure theory*, McGraw-Hill, Inc. 1989.

13. Frank Jensen, Introduction to Computational Chemistry (John Wiley & Sons Ltd 1999).

14. George J. Kavarnos, Fundementals of Photoinduced Electron Transfer (VCH Publishers, Inc. 1993) Figure 1.3 p.5.

15. P. Hohenberg, W. Kohn, Phys. Rev. B, 136, 864 (1964).

16. R. G. Parr and W. Yang, Density Functional Theory of Atoms and Molecules, Oxford Univ. Press, Oxford (1989).

18. Erich Runge and E. K. U. Gross, Phys. Rev. Lett. 52, 977 (1984).

19. M. A. L. Marques and E. K. U. Gross, Ann. Rev. Phys. Chem., 55, 427 (2004).

20. R. Eric Startmann, Gustavo E. Scuseria, Michael J. Frisch, J. Chem. Phys., 109, 8218 (1998).

21. U. Lourderja, Manoj K. Harbola, N. Satyamurthy, Chem. Phys. Let., 366, 88 (2002).

22. Maurizio Cossi and Vincenzo Barone, J. Chem. Phys., 98, 4708 (2001).

23. J.-L. Pascual-Ahuir, E. Silla, and I. Tuñon, J. Comput. Chem. 15, 1127 (1994).

25. Mikael P. Johansson and Dage Sundholm, J. Chem. Phys., 120, 3229 (2004).

26. Nobuyuki Matsuzawa, Masafumi Ata, David A. Dixon, J. Phys. Chem., 99, 7698 (1995).

28. W. Robert Scheidt, The Porphyrin Handbook , K.M. Kadish, K.M. Smith, R. Guilard, Eds. Vol. 3, Academic Press (1999).

29. Claude Lecomte, Marie-Madeleine Rohmer, Mark Bénard, The Porphyrin Handbook, K.M. Kadish, K.M. Smith, R. Guilard, Eds. Vol. 7, Academic Press (1999).

30. Axel D. Becke, J. Chem. Phys., 98, 5648 (1993).

31. Jesus M Ugalde, Barry Dunietz, Andreas Dreuw, Martin Head-Gordon, Russell J. Boyd, J. Phys. Chem. A, 108, 4653 (2004).

32. Harold J. Harmon and Mammadur Rahaman, private communication (2005).

33. Harold J. Harmon, private communication (2005).

34. Hiroshi Kobayashi and Yasuo Yanagawa, Bull. Chem. Soc. Jpn., 45, 450 (1972).

35. W. Blau, H. Byrne, W. M. Dennis, Optics Comm., 45, 25 (1985).

36. Fei Hao-Sheng, Han Li, Ai Xi-cheng, Yin Rui, Shen Jia-Cong, Chin. Sci. Bull., 37, 4 (1992).

37. Dayle M. Smith, Michel Dupuis, T.P. Straatsma, Mol. Phys., 103, 273 (1985).

38. George J. Kavarnos, Fundementals of Photoinduced Electron Transfer (VCH Publishers, Inc. 1993).

40. George J. Kavarnos, Fundementals of Photoinduced Electron Transfer (VCH Publishers, Inc. 1993) Figure 1.20 p.32.

41. George J. Kavarnos, Fundementals of Photoinduced Electron Transfer (VCH Publishers, Inc. 1993) Figure 1.22 p.38.

42. D. Rehm and A. Weller, Isreali J. Chem., 8, 259 (1970).

43. Patrick S. Mariano, Adv. in Elec. Trans. Chem. (JAI Press INC. 1993).

44. Ming-Ju Huang and Jerzy Lszczynski, Theo. Chem., 592, 105 (2002).

45. Harold J. Harmon and Mammadur Rahman, Private communication (2005).

46. Dillon Scofield, Private communication (2006).

VITA

Clint B. Conner

Candidate for the Degree of

Doctor of Philosophy

Thesis: THEORETICAL STUDIES OF EXCITED STATE ELECTRON TRANSFER BETWEEN IRON-PORPHYRIN AND TRINITRO-TOLUENE

Major Field: Physics

Biographical:

Personal Data: Born in Tulsa, Oklahoma, on February 12, 1977, the son of Mark Conner and Debi Foster.

Education: Graduated from Claremore High School, Claremore, Oklahoma in May 1995; received Associates of Science degree in Mathematics from Rogers State University, Claremore, Oklahoma in July 1998. Received Bachelor of Science degree in Engineering Physics from Northeastern State University, Tahlequah, Oklahoma in December 2000. Completed the requirements for the Doctor of Philosophy degree with a major in Physics at Oklahoma State University in December 2006.

Professional Memberships: American Physical Society.

Name: Clint B. Conner Date of Degree: December, 2006

Institution: Oklahoma State University Location: Stillwater, Oklahoma

Title of Study: THEORETICAL STUDIES OF EXCITED STATE ELECTRON TRANSFER BETWEEN IRON-PORPHYRIN AND TRINITROTOLUENE

Pages in Study: 75 Candidate for the Degree of Doctor of Philosophy

Major Field: Physics

Scope and Method of Study: The purpose of this study was to find and better understand the degradation of trinitrotoluene (TNT) by way of the photocatalyst iron-tetraphenyl-porphyrin-sulfonate (FeTPPS) by looking at a possible pathway in which the process might proceed. We studied a smaller iron complex iron-porphyrin (FeP), due to the complexity of the larger molecule in terms of size, to determine if future calculations involving FeTPPS could be handled more effectively using the much smaller FeP. We used various levels of theory in order to determine the viability of the process studied, and made use of our computer cluster to carry out the necessary calculations.

Findings and Conclusions: Using FeTPPS as a photocatalyst has been shown to degrade or deactivate TNT experimentally. The analysis of our FeP system has given us the theoretical excited state spectrum which is in good agreement with that of the experimental spectrum. We calculated the different multiplets of the iron complexes and found near degeneracies amongst the ground states. This analysis shows a mixing of the multiplets in the system and that the excitation of the iron complexes utilizes both the triplet and the quintet states. With the good agreement between the theoretical results and the experimental results we found that using the smaller iron complex FeP, we can account for the same behavior as that of the larger iron complex FeTPPS. We then analyzed the thermodynamics of the process to determine the if the degradation process would run. We did find that the pathway studied is certainly a possibility in which the process can take. Therefore, we showed that we can use the smaller iron complex to model a similar but larger iron complex, and that the process is thermodynamically favored with the pathway we studied.

ADVISOR'S APPROVAL Dr. Timothy M. Wilson